Chapter 3: Mechanistic insights on catalytic oxidation of NO to NO_2 on $[Pt_2]^{0,\pm}$ monometallic dimers using O_2

Abstract

A comprehensive density functional theory (DFT) investigation of the catalytic oxidation of NO to NO_2 on neutral and charged $[Pt_2]^{0,\pm}$ dimers has been considered employing M06L/def2TZVP level of theory. Pt_2 dimers have been widely explored for diverse catalytic processes and reported to provide detailed information about the local chemistry of Pt and its electronic environment. Previous studies have shown that small Pt clusters can have similar NO adsorption behaviour as that of Pt surfaces, making their application more attractive. Single as well as co-adsorption energies of NO and O_2 molecules suggest that the traditional Langmuir Hinshelwood (LH) mechanism and less explored termolecular Eley-Rideal (TER) and termolecular Langmuir Hinshelwood (TLH) mechanisms, are suitable for a full catalytic reaction pathway in which two NO molecules are converted to two NO_2 molecules, initiated by an activated O_2 molecule. Activation barrier reveals that the TER mechanism is found to be more reliable in converting two NO molecules into two NO_2 molecules on $[Pt_2]^-$ dimer. In addition to shedding light on the intrinsic characteristics of Pt_2 dimers, the study will serve as a benchmark for investigating the oxidation process of NO to NO_2 utilizing models of termolecular chemical processes.

Graphical Abstract

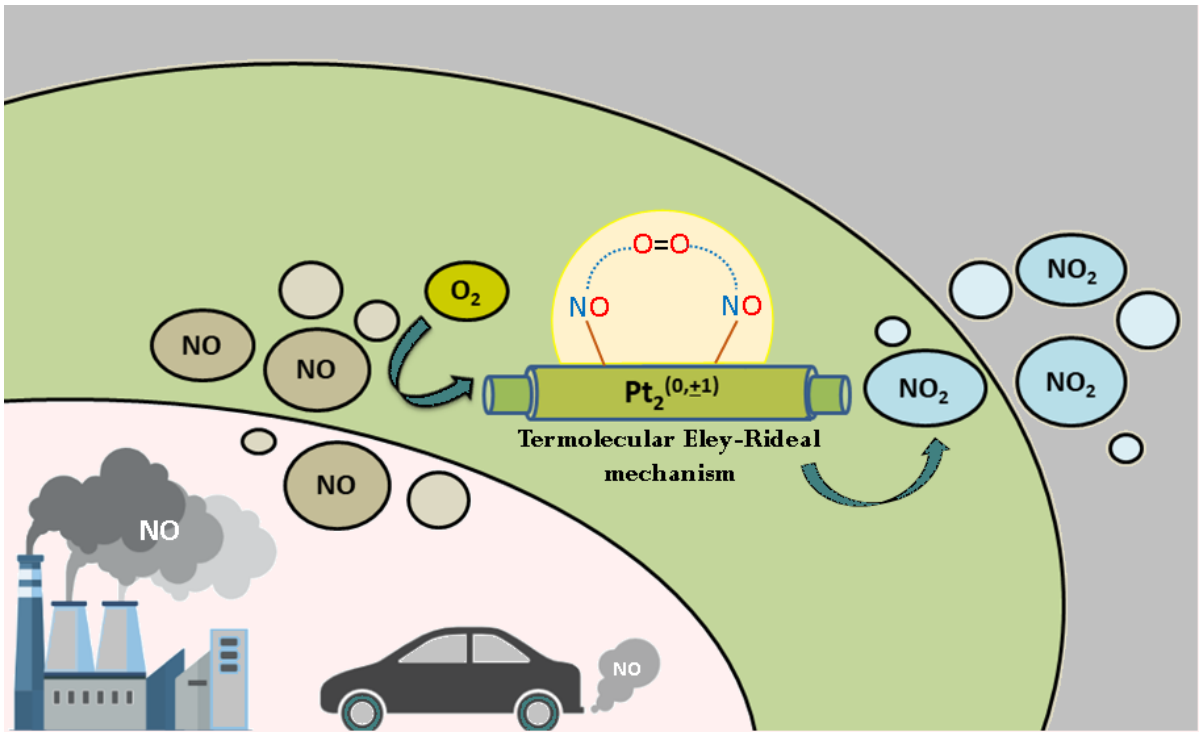

3.1 Introduction

Nitrogen oxides (NO_x) are one of the main air pollutants responsible for a variety of environmental issues, including acid rain, haze, and photochemical smog. Nitric oxide or nitrogen monoxide (NO) accounts for more than 90 percent of NO_x. It is a hazardous pollutant that gets released in the exhaust gas of diesel engines [1] and is the cause of serious respiratory ailments [2, 3]. Prior to emission, it is crucial to chemically convert NO to N_2 in order to prevent air pollution. Despite the apparent irony, the catalytic oxidation of NO is a crucial phase in its catalytic reduction. NO_x storage and reduction (NSR), continuously regenerating traps (CRT), and selective catalytic reduction (SCR) are modern techniques for NO reduction. In NSR, NO is oxidized into nitrogen dioxide (NO_2) and/or nitrate (NO_3) and temporarily retained on the surface of a noble metal before being reduced [4]. In CRT, NO is converted to NO_2, which then oxidizes unburnt hydrocarbons on a diesel particulate filter [5]. Also, the catalytic oxidation of NO is one of the most important steps in the Ostwald process for making nitric acid [6]. The catalytic oxidation of NO and NO_2 is thus established as a crucial reaction for the reduction of detrimental NO_x gases, and considerable effort has been put into developing efficient catalysts for NO oxidation.

Platinum is the predominant choice for catalytic oxidation of NO in all of these current approaches due to its high catalytic activity. It is regarded as the model catalyst for NO oxidation and has been extensively investigated in the past years [7-11]. The catalytic activity of platinum catalysts for NO oxidation under different feed containing NO and O_2 have been studied [7, 12]. Denton *et al.* [13] studied the oxidation rate of NO for both Pt/SiO_2 and Pt/Al_2O_3 and found out that Pt particle size was a key reason in controlling the reaction rate while the impact of the support was negligible. Schmitz *et al.* [9] investigated the impact of precursor, support, loading and processing conditions on NO oxidation over Pt catalysts. It was found that both Pt/Al_2O_3 and Pt/SiO_2 systems were exhibiting structure sensitivity. Because of its excellent catalytic activity even at 250°C, precious platinum metal is the best active component for NO oxidation. However, platinum-based catalysts are expensive, hence optimizing precious metal atomic efficiency is crucial.

Recently, experimentalists are exploring "nano" catalysis due to the strong reactivity of single metal atoms and/or low-atomicity clusters [14, 15]. Atomic clusters are ideal models [16-19] for understanding the complex catalytic reactions at the molecular level. Quantum chemistry simulations, in conjunction with state of the art mass spectrometry and spectroscopic studies, can aid in finding catalytically active sites in a cluster and clarifying the root cause of its reactivity.

Several experimental as well as theoretical studies on the reactivity of gas-phase Pt clusters have been performed in recent years, particularly in the field of oxidation catalysis. Fernandez *et al.* [20] investigated catalytic NO reduction with CO by subnanometric Pt clusters using a combination of IR spectroscopy and electronic structure calculations in which they found out that the Pt clusters are more reactive in comparison to singly dispersed Pt atoms. Weiss *et al.* [21] did isotopic and kinetic study for NO oxidation on supported Pt clusters in which they explored size effect of Pt clusters on NO oxidation and O_2 exchange rates. Schneider and his workers [22] did theoretical investigation of the effect of Pt cluster size on the oxidation of CO and NO and found out that the oxidation by molecular oxygen is thermodynamically more favorable compared to oxidation by atomic oxygen in Pt clusters. Narula *et al.* [23] did density functional theory for NO oxidation on single supported Pt atoms using modified Langmuir Hinshelwood mechanism in which they found out that NO oxidation activity decreases with the decreasing Pt particle size but accelerates when Pt is present only as single atom. Hamad *et al.* [24] have explored the stability of platinum clusters and adsorption of NO over it and established that small Pt clusters can provide similar NO adsorption behaviour as that of Pt surfaces which makes the application of Pt clusters more promising.

In general, NO oxidation on catalysts may occur via traditional Eley-Rideal (ER) [25] or Langmuir-Hinshelwood (LH) mechanism [26]. Recently, two new mechanisms namely termolecular Eley-Rideal (TER) [27, 28] and termolecular Langmuir-Hinshelwood (TLH) mechanism [29] have been proposed which are models of trimolecular chemical reactions. Based on the adsorption and co-adsorption properties of the reactants (NO and O_2), we propose for the first time NO oxidation using gas phase monometallic $[Pt_2]^{0,\pm}$ dimer catalyst in which the oxidation reaction proceeds via LH, TER and TLH mechanisms. The reason for

choosing Pt_2 dimers is that it has been extensively investigated for different catalytic reactions and reported to provide detailed information about the local chemistry of Pt and its electronic environment for such type of reactions [30-33]. Moreover, the charge on a catalyst plays a key role in tuning its reactivity [34-36]. Hence, neutral as well as charged Pt_2 dimers has been selected to find the suitable mechanistic pathways for NO oxidation. Till date, limited information is available for systematic investigation on the mechanistic details for NO oxidation on neutral and charged Pt_2 dimers. The investigation will not only provide information about the intrinsic features of Pt_2 dimers, but it will also serve as a point of reference for exploring oxidation process of NO to NO_2 using relatively less explored models of trimolecular chemical reactions.

3.2 Computational Details and Kinetic Theory

Gaussian 09 software package [37] is used to perform Density Functional Theory (DFT) calculations to obtain the lowest energy structures and thermochemical properties of the species involved in the reaction mechanism. A more popular local density M06L functional, developed by Zhao and Truhlar [38], is chosen for geometry optimizations and frequency calculations. The Minnesota M06L functional gives good results for both the main group and transition metals by establishing the dependency of the exchange-correlation energy on local spin density, spin density gradient, and spin kinetic energy density. A density-fitting triple-ζ valence with single polarization (def2TZVP) [39] basis set is employed to locate the atomic orbitals of the atoms. Critical bond dissociation energies of Pt-Pt, Pt-N and Pt-O bonds are calculated employing 15 different functionals along with density fitting triple-ξ def2TZVP basis set as shown in Table 3.1. Critical Bond dissociation energies (BDE) for Pt-Pt, Pt-N and Pt-O are calculated using the equations (1), (2) and (3) respectively-

$$BDE_{Pt-Pt} = 2 * E_{Pt} - E_{Pt-Pt} \quad (1)$$

$$BDE_{Pt-N} = E_{Pt} + E_N - (E_{Pt-N}) \quad (2)$$

$$BDE_{Pt-O} = E_{Pt} + E_O - (E_{Pt-O}) \quad (3)$$

Table 3.1: Benchmarking of 15 different functionals employing def2TZVP basis set with respect to experimental values of bond length, frequency and critical bond

dissociation energy (BDE) of Pt_2 dimer along with the BDE of Pt-N and Pt-O bond. The BDEs reported for Pt-N and Pt-O are computed with respect to Pt monomer.

Functionals	r_e (in Å)	ω_e (in cm^{-1})	BDE (in kJ/mol)		
			Pt-Pt	Pt-N	Pt-O
B3LYP	2.349	233	261.06	327.24	375.78
B3P86	2.323	244	279.41	346.61	395.32
B3PW91	2.327	242	268.63	323.30	377.87
HSEH1PBE	2.328	242	263.31	313.11	367.90
M06	2.369	224	263.68	289.63	354.42
M06L	2.363	222	309.84	343.17	403.60
M11L	2.383	209	175.50	262.08	353.42
M062x	2.308	249	133.97	294.16	294.16
mn12sx	2.320	249	300.11	337.63	383.66
mpw1pw91	2.321	245	251.76	303.43	360.12
PBE	2.345	231	345.80	431.61	472.04
PBE0	2.320	256	260.52	315.35	370.26
TPSS	2.339	236	333.39	392.60	435.89
TPSSh	2.330	241	299.72	348.39	397.59
wb97xd	2.475	188	171.79	305.11	369.01
Experimental	2.333 [40]	223 [40]	307±2 [41]	374±9.6 [41]	418±11.6 [41]

The best outcome is given by M06L in describing bond dissociation enthalpies of the bonds close to experimental data. Moreover, recent DFT studies [42-46] have also shown the dependability of the M06L functional on predicting and exploring the properties of precious metals accurately. While no imaginary frequency is seen for the reactant, intermediates, or products, the presence of a single imaginary frequency in the vibrational spectra validates the transition state. During the calculations, the transition state structure (TSs) is located using Berny algorithm [47] or the synchronous transit-guided quasi-Newton (STQN) method [48]. Intrinsic Reaction Coordinate (IRC) calculations [49] have been performed in order to check the reliability of the reaction path. An ultrafine integration grid is taken

into account for all the calculations. Thermochemistry such as enthalpy, entropy and free energy have been obtained from frequency calculations using the rigid rotor harmonic oscillator (RRHO) model at 298.15 K and 1 atm.

The adsorption energy (E_{ads}) of NO and O_2 on $[Pt_2]^{0,\pm}$ dimer has been calculated using the equation-

$$E_{ads} = E_{dimers/NO/O_2} - (E_{dimers} + E_{NO/O_2}) \quad (4)$$

where E_{dimers} represents the total zero-point corrected energy of the $[Pt_2]^{0,\pm}$ monometallic dimers, E_{NO/O_2} is the total zero-point corrected energy of the NO/O_2 molecule and $E_{dimers/NO/O_2}$ is the total zero-point corrected energy of the NO/O_2 adsorbed on monometallic dimers. We have performed basis set superposition error calculation [50] (for adsorption energies) using the counterpoise method and found the BSSE to be less than 1 kcal/mol. Since the adsorption energies are large, BSSE of <1 kcal/mol is typically negligible for chemisorption. Natural Bond Orbital (NBO) [51] calculations have been performed for the pure catalysts and the reactants at the same level of theory to look into their chemical behavior. Furthermore, orbital composition analysis is carried out using Multiwfn program [52] to find the composition of the HOMO-LUMO isosurface of the clusters.

Rate constant of each step in a catalytic oxidation reaction is obtained using well known kinetic theory, that is, Transition State Theory (TST) [53] and is usually expressed by the following relation:

$$k = \Gamma(T)\frac{k_B T}{h} e^{\left(\frac{-\Delta G^{TS}}{RT}\right)} \quad (5)$$

where $\Gamma(T)$ represents the transmission coefficient, which is obtained from the following expression:

$$\Gamma(T) = 1 + \frac{1}{24}\left(\frac{h\nu^{\#}}{k_B T}\right)^2 \quad (6)$$

In Eq.(5), ΔG^{TS} is the difference of Gibbs free energy values for TS and reactants. In Eq. (6), $\nu^{\#}$ is the magnitude of the imaginary frequency of the transition state (TS). Other terms retain their normal meaning.

3.3 Results and Discussion

3.3.1 Electronic structures and properties of $[Pt_2]^{0,\pm}$ catalyst

Ground state electronic structures of $[Pt_2]^{0,\pm}$, NO and O_2 along with their HOMO-LUMO isosurfaces obtained at the M06L/def2TZVP level of theory are shown in Figure 3.1 along with their bond lengths (in Å) and Mulliken charges (shown in parentheses). Neutral Pt_2 dimer has a ground state spin multiplicity (SM) of triplet, while cationic and anionic dimer have ground state spin multiplicities of quartet and doublet, respectively. For all the three dimers, HOMO and LUMO comes from the same spin channel {HOMO(β), LUMO(β)}. As shown in Figure 3.1, the bond lengths of $[Pt_2]^0$, $[Pt_2]^+$, $[Pt_2]^-$ are 2.363 Å, 2.503Å and 2.436 Å, respectively. The ground state spin multiplicity and the bond lengths are in good agreement with the previously reported results [40, 54]. The bond lengths of NO, O_2 and NO_2 are found to be 1.147 Å, 1.205 Å and 1.191 Å respectively which are almost equivalent to the bond length values reported in CRC handbook of chemistry and physics [41]. According to NBO calculations, each Pt atom in $[Pt_2]^0$ (SM=3) has a valence population of $6s^{1.06}$ $5d^{8.92}$ $6p^{0.02}$. With the addition of one positive charge $[Pt_2]^+$ (SM=4), the valence population of each Pt atom transforms to $6s^{0.69}$ $5d^{8.79}$ $6p^{0.02}$. Electrons are subsequently lost from both the 6s and the 5d orbitals. For anionic system $[Pt_2]^-$ (SM=2), extra electron is dispersed across the 6s and 5d orbitals ($6s^{1.21}$ $5d^{9.26}$ $6p^{0.02}$ $6d^{0.01}$) as a result of the additional negative charge. The orientation of HOMO-LUMO of the catalysts and the reactants are also depicted in Figure 3.1. The HOMO and LUMO orbitals of the clusters are of particular interest since they are directly involved in the reaction at hand. In $[Pt_2]^0$, the major contributor of HOMO is the d_z^2 orbitals of both the Pt atoms, contributing roughly 90%. The remaining part is contributed via 6s orbitals of each Pt atom. The LUMO of neutral Pt_2 is well distributed with equal contribution from d_{xz} orbitals of each Pt atom. For $[Pt_2]^+$, the main contributors for HOMO are d_{x2-y2} and d_z^2 from each Pt atom. In LUMO, 6s orbitals of each Pt atoms provide major contribution while d_{x2-y2} and d_z^2 contribute little. The major contributors of HOMO and LUMO for $[Pt_2]^-$dimer are d_{yz} and d_{xz} orbitals, respectively. The orbitals which are significantly contributing to the HOMO-LUMO of each cluster are listed in details in Table 3.2.

Table 3.2: Contribution of each orbital to the HOMO and LUMO of $[Pt_2]^{0,\pm}$ dimer (Major contributions are highlighted)

Cluster	Atom	Label	Type	Contribution
Pt_2_neutral (HOMO)	1Pt	s	6s	5.38%
	1Pt	d_{z2}	5d	44.45%
	2Pt	s	6s	5.33%
	2Pt	d_{z2}	5d	44.45%
Pt_2_neutral (LUMO)	1Pt	d_{xz}	5d	49.70%
	2Pt	d_{xz}	5d	49.70%
Pt_2_cation (HOMO)	1Pt	s	6s	0.88%
	1Pt	d_{x2-y2}	5d	36.81%
	1Pt	d_{z2}	5d	12.27%
	2Pt	s	6s	0.88%
	2Pt	d_{x2-y2}	5d	36.81%
	2Pt	d_{z2}	5d	12.27%
Pt_2_cation (LUMO)	1Pt	s	6s	31.99%
	1Pt	p_z	6p	0.50%
	1Pt	d_{x2-y2}	5d	7.45%
	1Pt	d_{z2}	5d	9.59%
	2Pt	s	6s	31.99%
	2Pt	p_z	6p	0.50%
	2Pt	d_{x2-y2}	5d	7.45%
	2Pt	d_{z2}	5d	9.59%
Pt_2_anion (HOMO)	1Pt	p_y	6p	0.65%
	1Pt	d_{yz}	5d	49.18%
	2Pt	p_y	6p	0.65%
	2Pt	d_{yz}	5d	49.18%
Pt_2_anion (LUMO)	1Pt	p_x	6p	0.52%
	1Pt	d_{xz}	5d	49.37%
	2Pt	p_x	6p	0.52%
	2Pt	d_{xz}	5d	49.37%

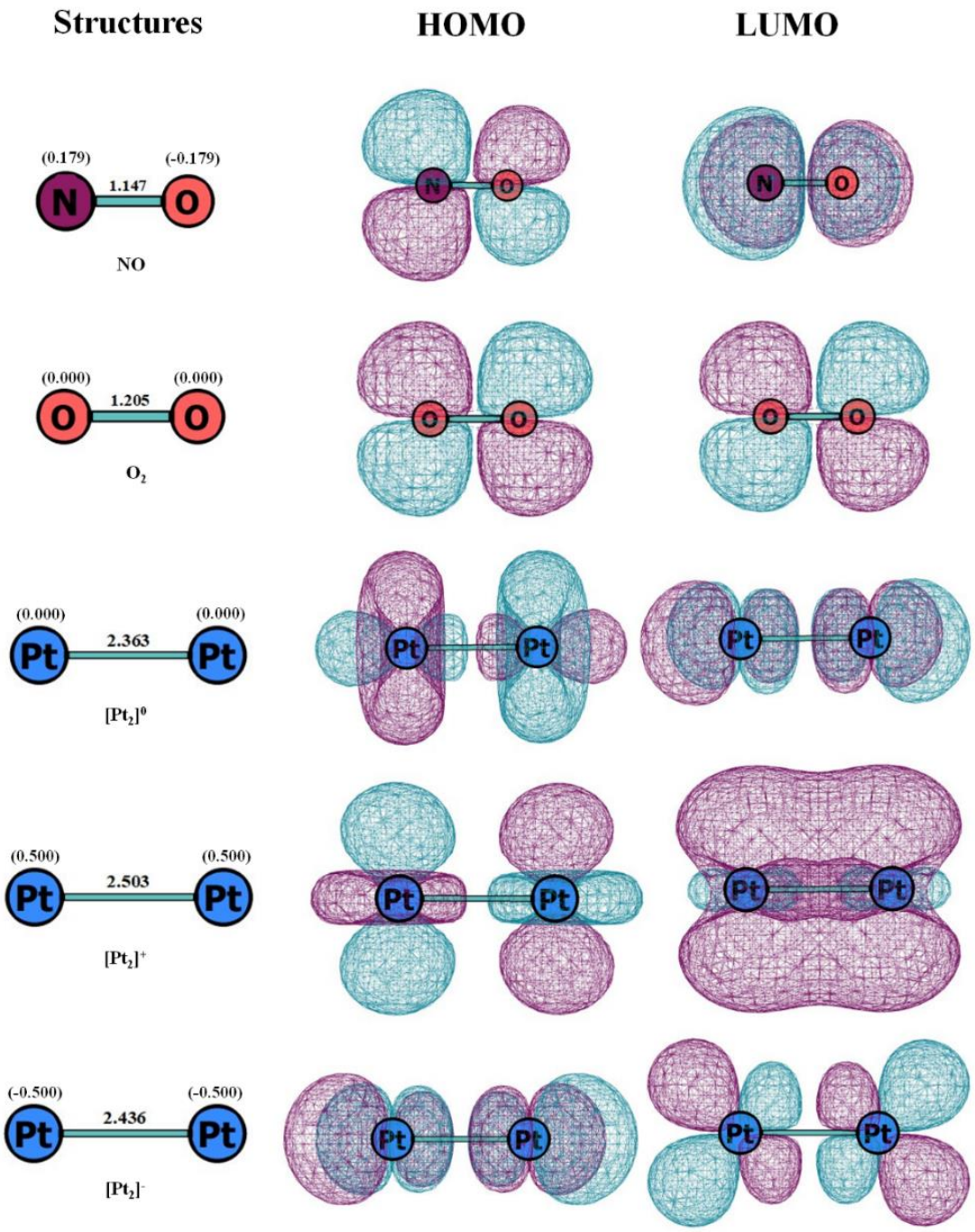

Figure 3.1: Optimized structures of NO, O_2 and $[Pt_2]^{0,\pm}$ dimers along with their HOMO-LUMO isosurfaces obtained at the M06L/def2TZVP level of theory.

Discussing electronic properties of each cluster are of significant importance as it provides valuable information about the chemical reactivity of the catalysts. Electronic properties of $[Pt_2]^{0,\pm}$ which includes HOMO-LUMO gap (HLG), Chemical Potential, Hardness, Softness and Electronegativity are given in Table 3.3.

Table 3.3: Electronic properties of $[Pt_2]^{0,\pm}$ dimer, (HLG=HOMO-LUMO gap) obtained at the M06L/def2TZVP level of theory.

Catalyst	Properties (in eV)				
	HLG	Hardness (η)	Softness (σ)	Chemical Potential (μ)	Electro-negativity (χ)
$[Pt_2]^0$	0.498	0.249	2.007	4.962	-4.962
$[Pt_2]^+$	0.344	0.172	2.902	11.537	-11.537
$[Pt_2]^-$	0.198	0.099	5.047	-1.099	1.099

Electronic properties such as hardness, softness, chemical potential, electronegativity can be determined using the frontier molecular orbitals. The equations are given below-

$$\eta = (E_{LUMO} - E_{HOMO})/2 \quad (7)$$

$$\sigma = 1/(2 * \eta) \quad (8)$$

$$\chi = (E_{LUMO} + E_{HOMO})/2 \quad (9)$$

$$\mu = -\chi \quad (10)$$

The HOMO-LUMO gap (HLG) is a necessary parameter for analyzing the electronic properties of a system. It is frequently associated with the chemical stability of clusters. A greater HLG value indicates greater inertness, whereas a lesser HLG value denotes greater reactivity. Chemical hardness is the measurement of a systems resistance to change in its electronic environment. It is related to HOMO-LUMO gap. Electronegativity is the measure of an atom or a molecule to attract a shared pair of electrons. Higher is the electronegativity, higher is the attraction towards electrons. Chemical potential is the negative of electronegativity (according to equation 10). The HLG of neutral Pt_2 is 0.498 eV, while its cationic and anionic counterparts have HLG values of 0.344 eV and 0.198 eV, respectively. Among the three dimers, the $[Pt_2]^-$ dimer is expected to be the most chemically reactive. Other electronic properties, such as hardness, softness, and chemical potential also indicating anionic Pt_2 dimer to be more reactive. However, these are

only preliminary assessments of the reactivity of a catalyst; and in order to draw a conclusion, one must examine the entire reaction mechanism which involves various intermediates and transition states.

3.3.2 Adsorption and co-adsorption of NO and O_2 on $[Pt_2]^{0,\pm}$ dimer

Adsorption analysis is the most efficient way for identifying a catalyst's active sites and the way reactants adhere to them. In order to activate the molecules, which in turn aid the reaction, an ideal or moderate contact is often needed between the reactants and the catalysts [55]. Most stable configurations of NO/O_2 adsorbed on $[Pt_2]^{0,\pm}$ dimers are shown in Figure 3.2 along with the bond parameters (in Å) and Mulliken charges (in parentheses). Calculated adsorption energies of NO/O_2 adsorbed on $[Pt_2]^{0,\pm}$ dimer are listed in Table 3.4.

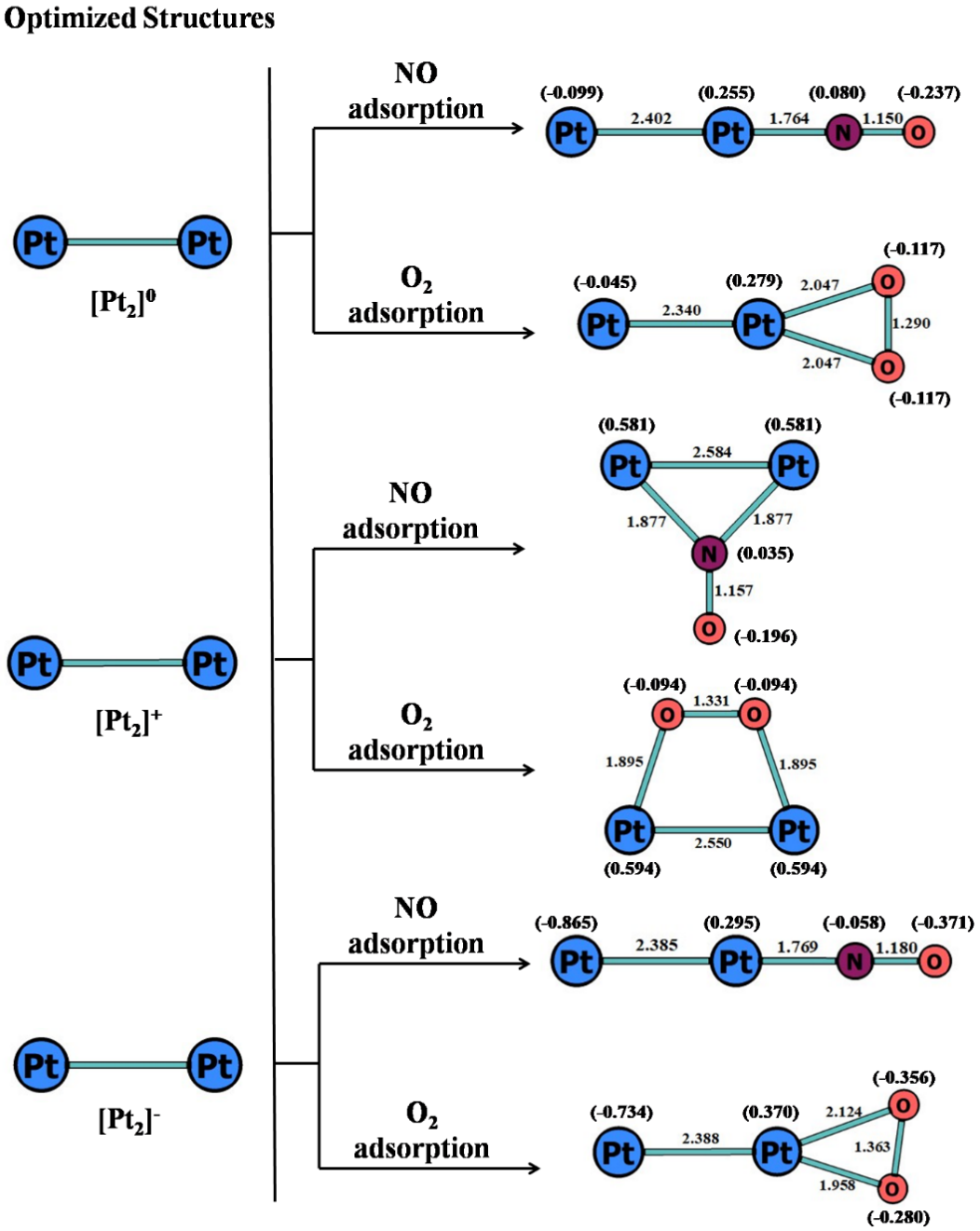

Figure 3.2: Optimized geometries of NO/O_2 adsorbed on $[Pt_2]^{0,\pm}$ dimer at M06L/def2TZVP level along with the bond parameters (in Å) and Mulliken charges (given in parentheses).

Table 3.4: Calculated adsorption energies (E_{ads}) (in kcal/mol) and vibrational frequencies (in cm^{-1}) of NO/O_2 adsorbed on $[Pt_2]^{0,\pm}$ dimer at M06L/def2TZVP level.

Catalyst	Spin	E_{ads} (NO)	υ_{Pt-N}	υ_{N-O}	Spin	E_{ads} (O_2)	υ_{Pt-O}	υ_{O-O}	Free υ_{N-O}	Free υ_{O-O}
$[Pt_2]^0$	2	-66.88	566.91	1939.57	3	-19.79	365.30	1218.28	1970.24	1645.64
$[Pt_2]^+$	1	-92.06	491.04	1829.95	2	-48.65	554.38	952.25	-	-
$[Pt_2]^-$	1	-81.24	563.27	1785.09	2	-42.76	531.04	992.31	-	-

Since Pt_2 is a monometallic dimer, it has active sites which are equivalent in nature. In neutral Pt_2 dimer, NO is adsorbed in an end-on position and its adsorption energy is found to be -66.88 kcal/mol (Table 3.4). The bond length and vibrational frequency of free NO molecule is 1.147 Å and 1970.24 cm^{-1}, respectively. After adsorption with $[Pt_2]^0$ dimer, the bond length of NO slightly increases to 1.149 Å whereas redshift in frequency takes place as the value decreases from 1970.24 cm^{-1} to 1939.57 cm^{-1}. The adsorption energy for NO on $[Pt_2]^+$ dimer is 92.06 kcal/mol which is the highest among the three catalysts. This is attributed to the adsorption of NO molecule in a bridged configuration on the $[Pt_2]^+$ catalyst. This fact is also reflected in the HOMO of $[Pt_2]^+$ dimer, as both metal centre possesses d_{x2-y2} orbital in HOMO which led NO to get adsorbed in bridging fashion. After adsorption, the frequency of NO is decreased and found to be 1829.95 cm^{-1} which indicates its activation after binding with the catalyst. In case of $[Pt_2]^-$ dimer, the adsorption energy for NO is -81.24 kcal/mol. However, activation of NO for anionic system is maximum as there is substantial increase in the bond length of NO (from 1.147 Å to 1.180 Å) and considerable redshift in frequency occurs for υ_{N-O} (decreases from 1970.24 cm^{-1} to 1785.09 cm^{-1}). Mulliken charges (as shown in Figure 3.2) of NO adsorbed on $[Pt_2]^-$ also shows that significant charge transfer has occurred from Pt to π* orbitals of NO. Table 3.5 provides Wiberg bond indices (WBIs) for single adsorption of NO and O_2 on $[Pt_2]^{0,\pm}$ dimers. WBIs is an effective tool which is used profoundly [56-58] to provide a comparative scale for the bond strength to predict the activated bonds that is most likely to break. The Wiberg bond order is one of the many approaches which quantify the bond order between atoms. The values are determined from Natural bond orbital (NBO) calculations. The NBO module reports

WBIs in the output. Among the three dimers, anionic system has the highest WBI values for the newly formed Pt-N bond (1.310 Å) and lowest for N-O bond (1.672 Å). This shows that the Pt-N bond order is found to be the highest and N-O bond order is found to be the lowest which also signifies highest back donation from d orbitals of Pt to π* orbitals of NO in case of $[Pt_2]^-$ dimer. However, cationic system has the highest adsorption energy despite the fact that activation of NO is found to be less as compared to anionic one. It may be due to the larger Pt-Pt bond distance in $[Pt_2]^+$, the NO has to maintain a larger bridged angle with the two Pt, as a result, Pt-N bond distance increases. Moreover, surface area is one of the major factor upon which the adsorption energy depends upon. In $[Pt_2]^-$ dimer, NO is adsorbed at the terminal position on one of the Pt atoms, while in cationic dimer, NO binds in a bridging fashion. In the bridged configuration, NO attains more active sites i.e. larger surface area to adsorb. Therefore, compared to energy released during a single adsorption at the terminal location, the energy released following the creation of two symmetrical bonds contributes more to the adsorption energy.

The activation of O_2 after binding with the catalyst is a vital step as it induces the reaction by reacting with NO. Free O_2 molecule has bond length of about 1.205 Å and vibrational frequency of 1645.64 cm^{-1}. For $[Pt_2]^0$ dimer, O_2 binds with one of the Pt atoms in a peroxide linkage form (also known as η^2 ligation) with adsorption energy of 19.79 kcal/mol. After adsorption, the bond length of O_2 increases from 1.205 Å to 1.290 Å whereas vibrational frequency decreases from 1645.64 cm^{-1} to 1218.28 cm^{-1} which indicates the activation of O_2 molecule adsorbed on the neutral dimer. It is to be noted that there is a direct correlation between the adsorption energies of O_2 and redshift in frequencies for O_2 ($\boldsymbol{\upsilon_{O-O}}$). The amount of redshift in frequency that occurs for O_2 is minimum on neutral Pt_2 (1645.64 cm^{-1} to 1218.28 cm^{-1}) whereas it is maximum for cationic Pt_2 (1645.64 cm^{-1} to 952.25 cm^{-1}). This is in parallel with the fact that the adsorption energy of O_2 is minimum for neutral Pt_2 (-19.79 kcal/mol) and maximum for cationic Pt_2 (-48.65 kcal/mol). It is further reflected by WBI value (Table 3.5) that the Pt-O bond interaction is strongest in case of the $[Pt_2]^+$ dimer while O-O bond interaction is the weakest as suggested above.

Table 3.5: Wiberg bond indices (WBIs) for single adsorption of NO and O_2 on $[Pt_2]^{0,\pm}$ dimer.

Adsorbed Species	Wiberg bond indices					
	$[Pt_2]^0$		$[Pt_2]^+$		$[Pt_2]^-$	
NO adsorbed	Pt-N	N-O	Pt-N	N-O	Pt-N	N-O
	1.295	1.852	0.848	1.850	1.310	1.672
O_2 adsorbed	Pt-O	O-O	Pt-O	O-O	Pt-O	O-O
	0.519	1.273	0.718	1.148	0.618	1.153

Even though, both nitrogen and oxygen atoms in NO are potential donors, it has been observed that NO binds with the catalysts using its Nitrogen atom in order to avoid large formal negative charge on a more electronegative oxygen atom. We have also observed that the value of adsorption energies of NO adsorbed on the dimers is more negative as compared to that of O_2 adsorbed on the same dimers. It is attributed to the fact that NO is a better π acceptor in comparison to that of O_2. It accepts electronic charge from metals to its antibonding π* orbitals, which in turn causes the strengthening of a metal-nitrogen bond as well as weakening of N-O bond.

Since both NO and O_2 are present in flue gas, it becomes important to check the various configurations of the co-adsorption of NO and O_2 molecules, two NO molecules as well as two O_2 molecules. Table 3.6 includes co-adsorption energies (Co-E_{ads}) (in kcal/mol) of NO and O_2, two NO and two O_2 molecules co-adsorbed on different sites of $[Pt_2]^{0,\pm}$ dimer at M06L/def2TZVP level of theory. The co-adsorption could occur at two adjacent Pt sites of dimer system or alternatively at the same single- Pt atom site. It is obvious from Table 3.6 that the adsorption on adjacent Pt sites is more suitable as compared to the adsorption at the same site. We have observed that the transfer of election density occur from catalyst to the reactants (NO and O_2) in a greater extend when they are adsorbed on adjacent sites of the catalyst. But when the reactants are adsorbed to the same atom, they are competing with each other for the electron transfer from the catalyst. However, both the adsorption configurations are important since they lead to two different

reaction routes (which is discussed in the subsequent sections). The co-adsorption modes of NO/O_2 and 2 NO adsorbed on neutral as well as charged Pt_2 dimers are shown in Figure 3.3 and 3.4, respectively. The co-adsorption energies of 2 O_2 adsorbed on $[Pt_2]^{0,\pm}$ dimer has been found to be the lowest among other co-adsorptions. Hence, the probability of two O_2 molecules adsorbed simultaneously on the dimers will be low and thus not discussed in detail.

Table 3.6: Calculated Co-adsorption energies (Co-E_{ads}) (in kcal/mol) of NO and O_2, two NO and two O_2 molecules co-adsorbed on different sites of $[Pt_2]^{0,\pm}$ dimer at M06L/def2TZVP level.

Catalyst	$[Pt_2]^0$		$[Pt_2]^+$		$[Pt_2]^-$	
	Spin	Co-E_{ads}	Spin	Co-E_{ads}	Spin	Co-E_{ads}
NO & O_2 (diff_Pt)	2	-67.66	3	-72.92	3	-80.49
NO & O_2 (same_Pt)	2	-65.00	3	-58.08	1	-69.37
2 NO (diff_Pt)	1	-96.18	2	-142.24	2	-126.46
2 NO (same_Pt)	3	-88.09	4	-105.25	2	-98.94
2 O_2 (diff_Pt)	3	-36.36	2	-42.82	2	-63.95
2 O_2 (same_Pt)	1	-21.06	2	-39.64	2	-50.48

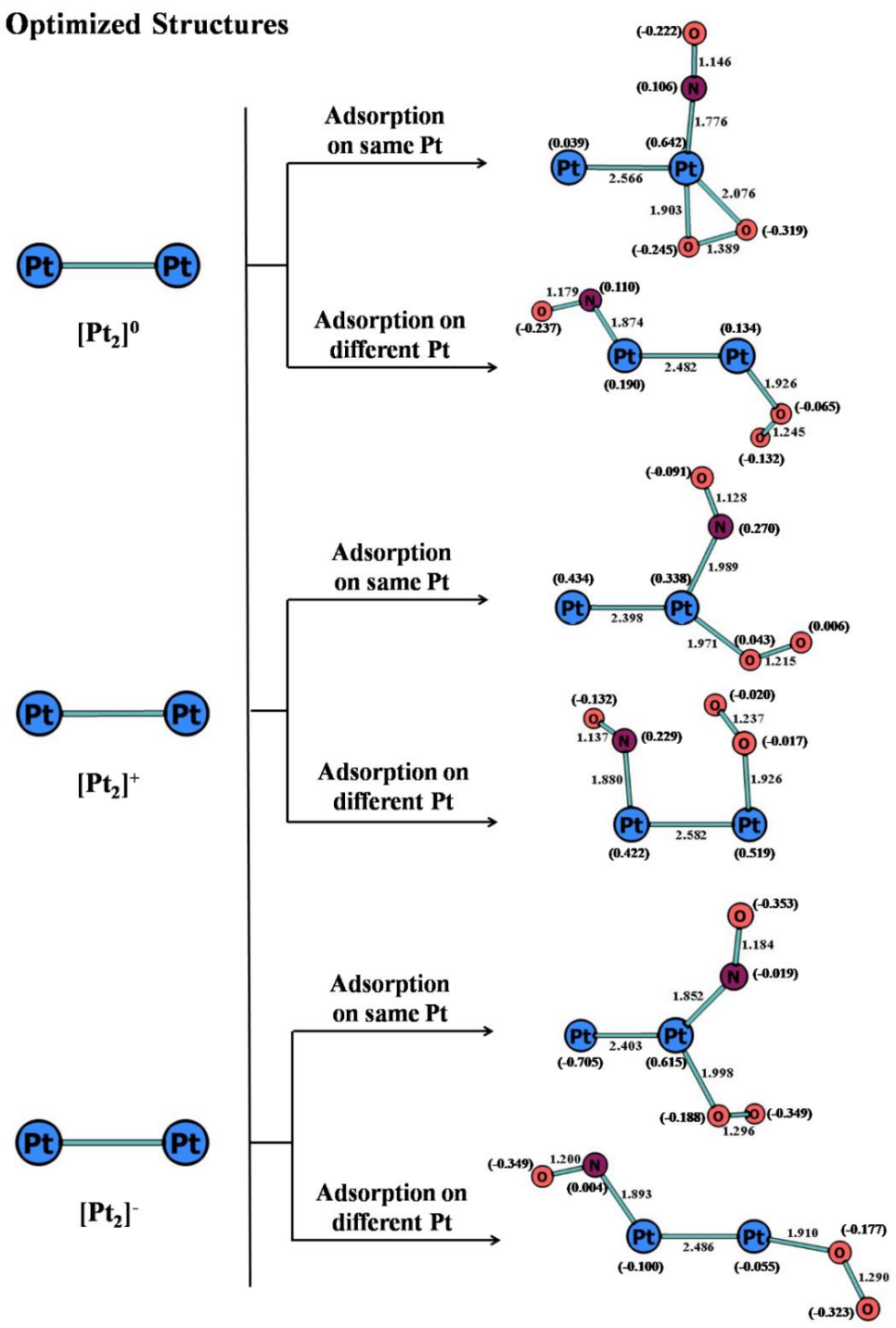

Figure 3.3: Optimized geometries of NO and O_2 co-adsorbed on $[Pt_2]^{0,\pm}$ dimers on different sites at M06L/def2TZVP level along with the bond parameters (in Å) and Mulliken charges (given in parentheses).

When it comes to the $[Pt_2]^0$ dimer, the energy difference between NO and O_2 co-adsorbed on separate Pt sites and the same Pt site is extremely minimal (2.66 kcal/mol). On the other hand, the co-adsorption energy difference of O_2 and NO for

different and same Pt sites in cationic and anionic systems is 11.12 kcal/mol and 14.84 kcal/mol, respectively. When examining the two co-adsorbed structures of $[Pt_2]^0$ dimer (Figure 3.3), bond lengths and Mulliken charges clearly show that O_2 is more active in the cases when NO and O_2 are co-adsorbed on the same Pt site. The charges 'q' for bonded O atoms in the same site adsorption are -0.245e and -0.319e whereas for adsorption on different sites, O atoms have -0.065e and -0.132e charges which signifies more charge transfer on O_2 molecule for same site adsorption with NO. Table 3.7 contains vibrational frequencies (in cm^{-1}) and WBIs for co-adsorption of NO and O_2 on $[Pt_2]^{0,\pm}$ dimer. Table 3.7 makes it evident that activation of both NO (1970.24 cm^{-1} to 1658.83 cm^{-1}) and O_2 (1645.64 cm^{-1} to 1353.95 cm^{-1}) occurs to some degree when NO and O_2 are co-adsorbed on distinct sites. This indicates that charge is transferred from Pt orbitals to both the reactants proportionately. On the other hand, when co-adsorbed on the same Pt atom, O_2 is significantly activated (1645.64 cm^{-1} to 969.25 cm^{-1}), whereas NO is barely activated (1970.24 cm^{-1} to 1960.28 cm^{-1}) indicating that charge transfer has taken place from Pt orbitals to antibonding π* orbitals of O_2 rather than NO. The value of WBIs is also supporting the above conclusion. In case of $[Pt_2]^+$, the activation of both the reactants are somewhat less in comparison to $[Pt_2]^0$. Looking at the Mulliken charges on the adsorbed reactants for both the configurations, it is evident that very little charge transfer has occurred to antibonding orbitals of the reactants. The WBI values for N-O and O-O bond for both the configurations are highest for $[Pt_2]^+$ which means both NO and O_2 are less activated when co-adsorbed on the cationic system. It is due to the fact that cationic dimer has overall +1 charge which makes it an electron deficient system. Hence, it becomes difficult for $[Pt_2]^+$ dimer to transfer electronic charges to antibonding orbitals of the reactants. However, the same is not the case for anionic $[Pt_2]^-$ dimer where backbonding to π* orbitals of NO and O_2 is comparatively easy since the metal centres bears a large electron density on their bonding orbitals. For co-adsorption on the same site, the Mulliken charges for 'N' and 'O' atoms of NO are -0.019e and -0.353e, respectively while O atoms of O_2 have charges of -0.188e and -0.349e. There is redshift in frequency for NO (1970.24 cm^{-1} to 1699.40 cm^{-1}) as well as O_2 (1645.64 cm^{-1} to 1170.36 cm^{-1}). Both Mulliken charges and vibrational frequencies show indications of backbonding from Pt-filled orbitals to NO and O_2-antibonding orbitals. The same is true for NO and O_2 co-

adsorbed on distinct Pt sites, which exhibit a redshift in frequency for both NO (1567.76 cm^{-1}) and O_2 (1191.10 cm^{-1}).

Table 3.7: Vibrational frequencies (in cm^{-1}) and Wiberg bond indexes (WBI) for co-adsorption of NO and O_2 on different Pt sites of $[Pt_2]^{0,\pm}$ dimer.

NO-O_2 co-adsorbed (Diff Pt)	**Vibrational Frequency (in cm^{-1}) and Wiberg bond index**					
	$[Pt_2]^0$		**$[Pt_2]^+$**		**$[Pt_2]^-$**	
	υ_{N-O}	**WBI_{N-O}**	**υ_{N-O}**	**WBI_{N-O}**	**υ_{N-O}**	**WBI_{N-O}**
	1658.83	1.856	1910.92	2.030	1567.76	1.763
	υ_{O-O}	**WBI_{O-O}**	**υ_{O-O}**	**WBI_{O-O}**	**υ_{O-O}**	**WBI_{O-O}**
	1353.95	1.347	1316.01	1.413	1191.10	1.317
NO-O_2 co-adsorbed (Same Pt)	**$[Pt_2]^0$**		**$[Pt_2]^+$**		**$[Pt_2]^-$**	
	υ_{N-O}	**WBI_{N-O}**	**υ_{N-O}**	**WBI_{N-O}**	**υ_{N-O}**	**WBI_{N-O}**
	1960.28	1.862	1952.01	2.139	1699.40	1.732
	υ_{O-O}	**WBI_{O-O}**	**υ_{O-O}**	**WBI_{O-O}**	**υ_{O-O}**	**WBI_{O-O}**
	969.25	1.110	1461.13	1.494	1170.36	1.291

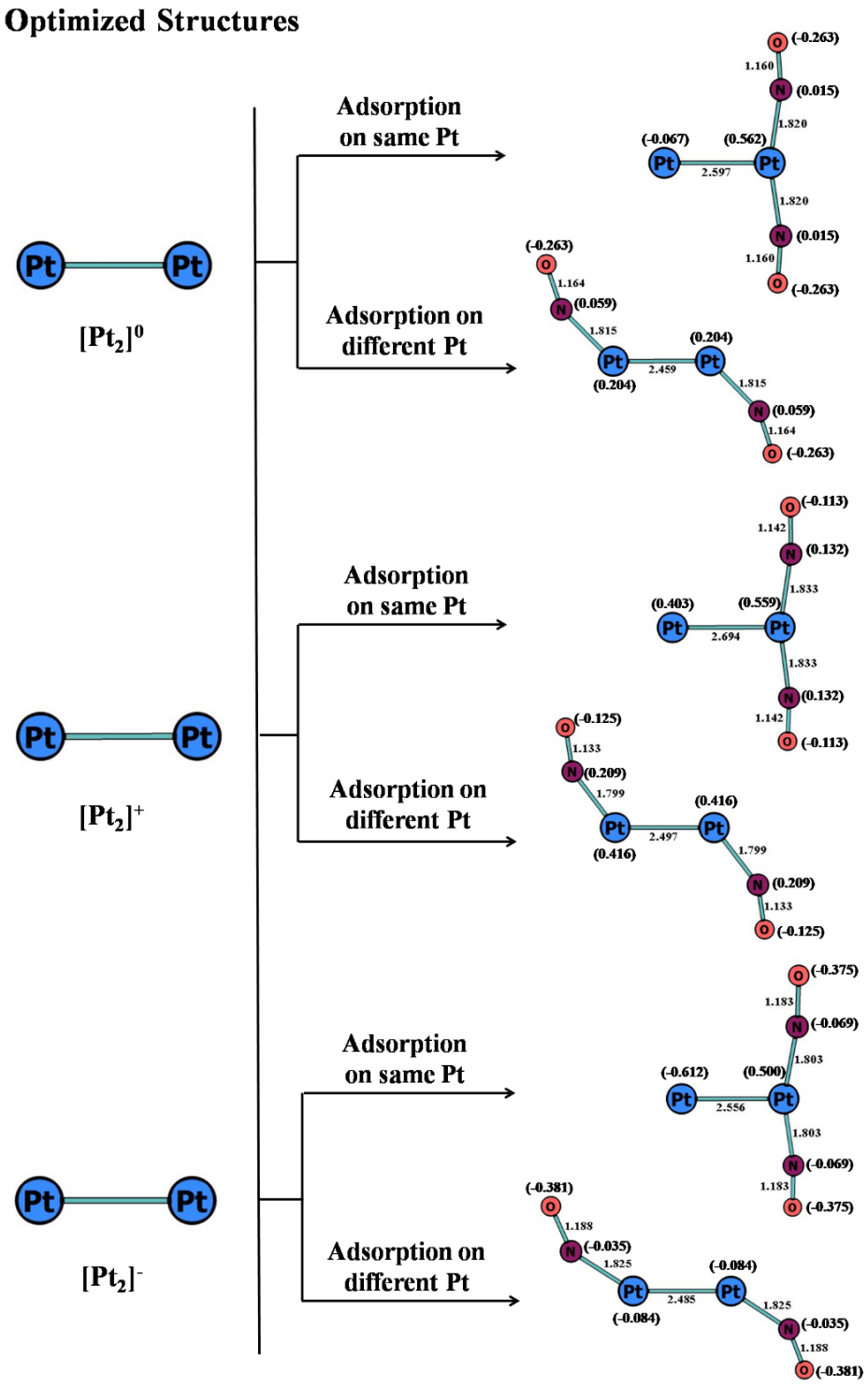

Figure 3.4: Optimized geometries of 2 NO co-adsorbed on $[Pt_2]^{0,\pm}$ dimers on different sites at M06L/def2TZVP level along with the bond parameters (in Å) and Mulliken charges (given in parentheses).

The energy difference between two NO molecules co-adsorbed on different Pt sites and the same Pt site for the $[Pt_2]^0$ dimer is 8.09 kcal/mol. For cationic and

anionic systems, the co-adsorption energy difference of two NO molecules when adsorbed on separate and same Pt sites is 36.99 kcal/mol and 27.52 kcal/mol, respectively. For co-adsorption on same site of $[Pt_2]^0$ dimer, looking at the Mulliken charge of Pt atom (0.562e), it is evident that some of the electron density has transferred from Pt to π* orbital of NO. As a result, elongation of NO occurs which is evident from its bond lengths (1.160 Å) and υ_{N-O} (1893.47 cm^{-1}). Similar is the case for co-adsorption at different sites where both the Pt atoms have charges 0.204e. This suggests some amount of electron transfer occurring from Pt to π* orbital of NO. Bond lengths (1.164 Å) and vibrational frequencies (1840.80 cm^{-1}) are also suggesting activation of NO. In case of cationic $[Pt_2]^+$ dimer, as it is an electron deficient system, the back-donation will be reduced as compared to its neutral counterpart. The bond lengths and vibrational frequencies show that the activation of NO is minimal for both configurations in $[Pt_2]^+$ dimer (Figure 3.4). Moreover, there is a blueshift in frequencies occurring for υ_{N-O} (1970.24 cm^{-1} to 1994.83 cm^{-1} (Different Pt) and 1980.28 cm^{-1} (Same Pt)) in both the configurations which suggests that the transfer of electron density from antibonding orbital of NO to vacant orbitals of Pt. This resulted in increase in bond order of NO as well as vibrational frequency. For $[Pt_2]^-$ dimer, the activation of NO is maximum. For co-adsorption at different Pt site on $[Pt_2]^-$ dimer, υ_{N-O} value is 1710.83 cm^{-1} and its corresponding WBI value is 1.675 (Table 3.8). While for co-adsorption at the same Pt site, υ_{N-O} value is 1786.21 cm^{-1} and its corresponding WBI value is 1.648. The values are suggesting that activation of NO is more in case of $[Pt_2]^-$ dimer as compared to its cationic and neutral counterparts. The value of co-adsorption energies of two NO molecules adsorbed on the dimers is more negative as compared to the co-adsorption energies of NO and O_2 adsorbed on the same dimers. The reason may lie in the fact that NO is a better π acceptor than that of O_2.

Table 3.8: Vibrational frequencies (in cm^{-1}) and Wiberg bond indexes (WBI) for co-adsorption of 2 NO molecules on different Pt sites of $[Pt_2]^{0,\pm}$ dimer.

2 NO co-adsorbed (Diff Pt)	**Vibrational Frequency (in cm^{-1}) and Wiberg bond index**					
	$[Pt_2]^0$		**$[Pt_2]^+$**		**$[Pt_2]^-$**	
	υ_{N-O}	**WBI_{N-O}**	**υ_{N-O}**	**WBI_{N-O}**	**υ_{N-O}**	**WBI_{N-O}**
	1840.80	1.804	1994.83	2.023	1710.83	1.675

2 NO co-adsorbed (Same Pt)	$[Pt_2]^0$		$[Pt_2]^+$		$[Pt_2]^-$	
	υ_{N-O}	WBI_{N-O}	υ_{N-O}	WBI_{N-O}	υ_{N-O}	WBI_{N-O}
	1893.47	1.786	1980.28	1.944	1786.21	1.648

The value of single adsorption energies of NO adsorbed on the dimers is much higher as compared to that of O_2 which means that the probability of reaction occurring via Eley-Rideal mechanism is very low. Based on the greater NO and O_2 co-adsorption energies on all three dimers, the Langmuir Hinshelwood (L-H) mechanism has been taken into consideration over Eley-Rideal mechanism. Additionally, the co-adsorption of two NO molecules give rise to two trimolecular reactions; Termolecular EleyRideal (TER) and Termolecular Langmuir Hinshelwood mechanism (TLH). In TER, two NO molecules are co-adsorbed on the catalyst and the other reactant, O_2 reacts directly from the gas phase. While TLH means all the three molecules (2 NO and O_2) are co-adsorbed onto the catalyst and will react simultaneously. Considering Table 3.6, we conclude that the co-adsorption of two NO molecules is more favourable in all the three dimers, whereas the probability of two O_2 molecules co-adsorbing on dimers is extremely low. Comparing our adsorption energies with more recent studies [59-63] have shown us that our calculations are reliable and efficient. The probability of reactions occurring via trimolecular reactions is higher given that the co-adsorption of two NO molecules are more favourable in all the three dimers. Therefore, L-H, TER and TLH mechanisms are taken into account for catalytic oxidation of NO to NO_2 on $[Pt_2]^{0,\pm}$ dimers.

3.3.3 Catalytic oxidation pathway of NO on $[Pt_2]^{0,\pm}$ dimers

3.3.3.1 Langmuir Hinshelwood (L-H) mechanism

Optimum adsorption of reactants onto the catalysts is an important step as it tends to activate the adsorbate molecules, which in turn, facilitate the reaction mechanism. In case of NO oxidation, activation of both the reactants (NO and O_2) is required as they interact with each other to facilitate the formation of NO_2. Langmuir Hinshelwood (L-H) mechanism is taken into account looking into the high co-adsorption energies of both the reactants. Previous studies have also reported

NO oxidation occurring via Langmuir Hinshelwood (L-H) mechanism [46, 64-65]. The initial co-adsorption of NO and O_2 molecules could occur at adjacent Pt atoms or alternatively at the same single-Pt atom site which results in reaction mechanism occurring via two reaction routes, named LH-1 and LH-2, respectively.

Formation of first NO_2 molecule is facilitated by molecular O_2 while formation of second NO_2 is assisted by atomic oxygen (O). The whole LH-1 mechanism undergoes via two steps: (i) Interaction of NO and O_2 and formation of NO_2 via breaking of O-N-O-O bond (TS1) and (ii) Incoming of second NO and formation of the second NO_2 (TS2). LH-2 mechanism on the other hand undergoes via three steps: (i) Interaction of NO and O_2 and formation of O-N-O-O bond (TS1) (ii) Breaking of the newly formed O-N-O-O bond and formation of first NO_2 (TS2) and (iii) Incoming of second NO and formation of the second NO_2 (TS3).

Figure 3.5(a), (b) and (c) demonstrate, respectively, the optimized geometries of intermediates and transition states involved in the catalytic oxidation pathway of NO via LH-1 on $[Pt_2]^0$, $[Pt_2]^+$, and $[Pt_2]^-$ dimers. The potential energy profile for the LH-1 mechanism on $[Pt_2]^{0,\pm}$ dimers has also been shown in Figure 3.6. The relative Gibbs' free energies of all the intermediates and transition states have been calculated with respect to $[Pt_2]^{0,\pm}$ dimers + 2NO (gas) + O_2 (gas) at 298K and 1 atm. The reaction mechanism starts with the co-adsorption of NO and O_2 on the alternative Pt atoms of neutral, cationic and anionic dimers, forming IM1n, IM1c and IM1a, respectively (n=neutral, c=cationic and a=anionic). For $[Pt_2]^0$ dimer, reaction is initiated when one O atom of adsorbed O_2 attacks the N atom of the NO adsorbed on the adjacent Pt atom, leading to the transition state TS1n with an imaginary frequency of 330.42***i*** cm^{-1}, in which the O-O bond is elongated from 1.254 Å to 1.674 Å and the distance between the N atom of NO and O atom of O_2 decreases to 1.330 Å. From the energy analysis, it is found that the energy barrier for TS1n is 36.67 kcal/mol, which makes it relatively difficult to occur at room temperature. In TS1c, elongation of O-O bond takes place (1.237 Å to 1.689 Å) and a new N-O bond (1.299 Å) is formed. The activation barrier associated with TS1c is 16.74 kcal/mol, and the reaction step is exothermic by 3.01 kcal/mol, which is feasible at room temperature. The same step follows for TS1a, where elongation of O-O bond takes place (1.290 Å to 1.589 Å) and the formation of a fresh N-O bond takes place. TS1a

has an activation barrier of about 40.48 kcal/mol which is quite high. Among the three transition states, TS1c has the lowest barrier height for the formation of first NO_2. It is clear from looking at the structure of IM1c that NO and O_2 that have been adsorbed to nearby Pt atoms are closer to one another. Therefore, NO and O_2 require less energy to reorganise their orbitals in order to react. The same is not the case for IM1n and IM1a, where there is a considerable gap between NO and O_2 molecules that have been adsorbed adjacently. As a result, both molecules require considerable orbital rearrangement energy to react, which is evident by their high activation barriers. After TS1, the O-O bond of the adsorbed O_2 is completely broken, resulting in the formation of first NO_2 and a residual O atom in IM2 for neutral as well as charged Pt_2 dimers. Removal of first NO_2 from the system results in the formation of Pt_2-O species named as IM3 (IM3n, IM3c and IM3a for neutral, cationic and anionic respectively). Reaction proceeds further when second NO enters the system and interacts with IM3, forming IM4 intermediate which is more stable than IM3 by 53.63 kcal/mol (IM4n), 49.61 kcal/mol (IM4c) and 46.10 kcal/mol (IM4a), respectively. The reaction is carried forward via TS2 where the lone O atom attacks the N atom of adjacent NO, to form the second NO_2 molecule. The bond distance between N atom of NO and adjacent O atom (1.773Å) shows the interaction between them. This step has activation energy of 41.37 kcal/mol and an imaginary frequency of 362.01***i*** cm^{-1} for neutral TS2n. Cationic TS2c has a barrier height of 24.13 kcal/mol, whereas anionic TS2a has a barrier height of 51.76 kcal/mol. 217.08***i*** cm^{-1} and 300.15***i*** cm^{-1} are the only imaginary frequencies for TS2c and TS2a, respectively. As with the first TS, the $[Pt_2]^+$ dimer also possesses the lowest barrier height for the formation of second NO_2 compared to its neutral and anionic counterparts. The reason for this is that the distance between NO and O, which are adjacently adsorbed, is considerably large (can be observed in IM4n and IM4a). Therefore, a great deal of energy is required to bring them close enough to react and form the product. However, in IM4c, second NO is adsorbed in a bridged manner between the two Pt atoms which makes it readily available to react with 'O' atom, to form NO_2. One important conclusion after performing the whole LH-1 mechanism has been found that the spin is conserved throughout the whole reaction. In $[Pt_2]^0$ dimer, LH-1 undergoes via SM=2 whereas in both the cationic and anionic dimer, LH-1 undergoes via SM=1.

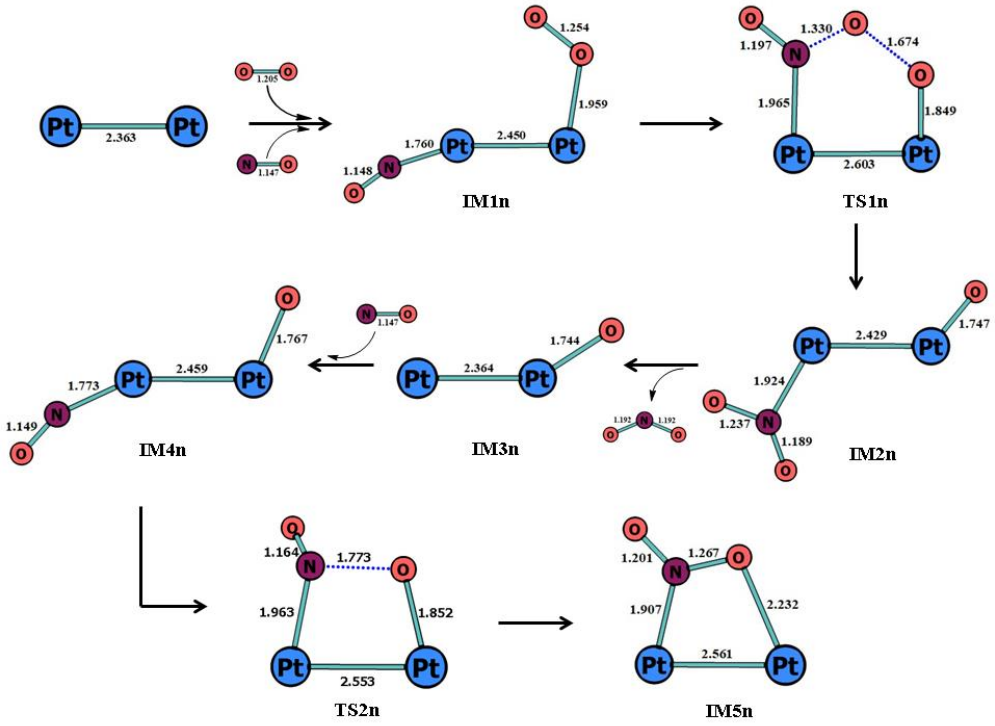
IM1n
TS1n
IM2n
IM3n
IM4n
TS2n
IM5n

(a)

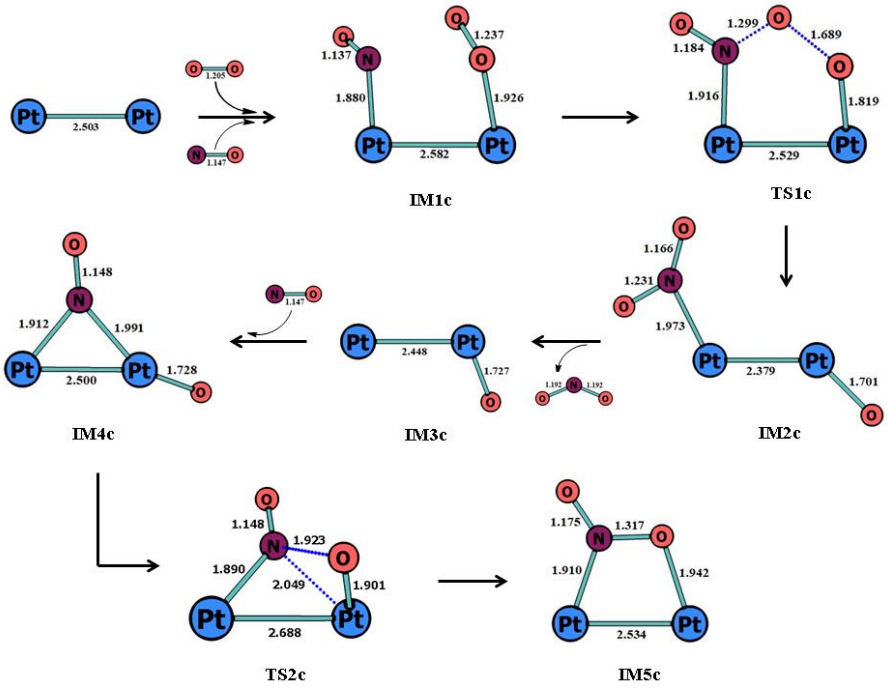
IM1c
TS1c
IM2c
IM3c
IM4c
TS2c
IM5c

(b)

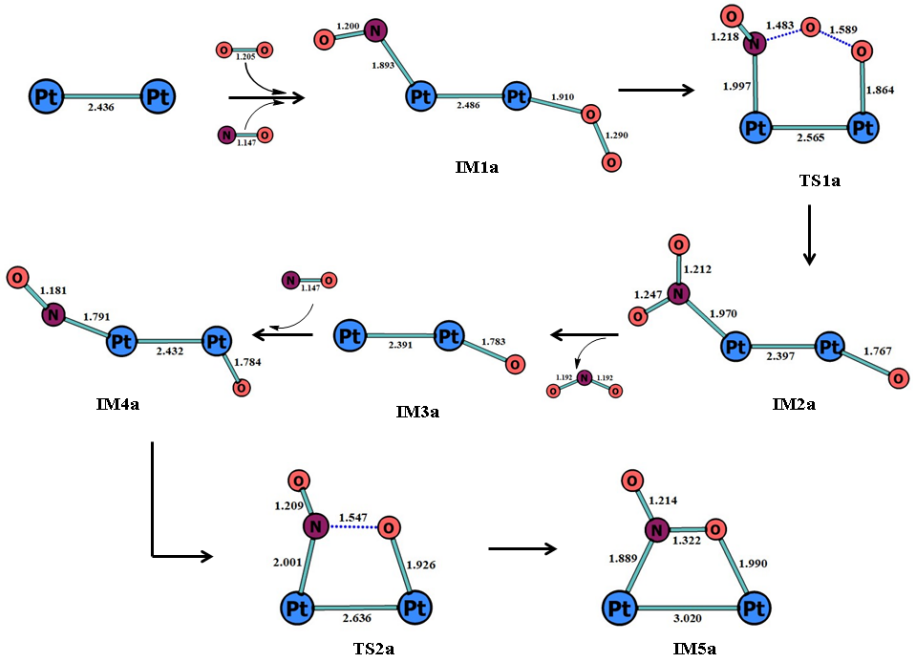

(c)

Figure 3.5: Optimized geometries of intermediates and transition states involved in catalytic oxidation pathway of NO via LH-1 mechanism on (a) $[Pt_2]^0$ dimer (b) $[Pt_2]^+$ dimer and (c) $[Pt_2]^-$ dimer along with their bond lengths (in Å).

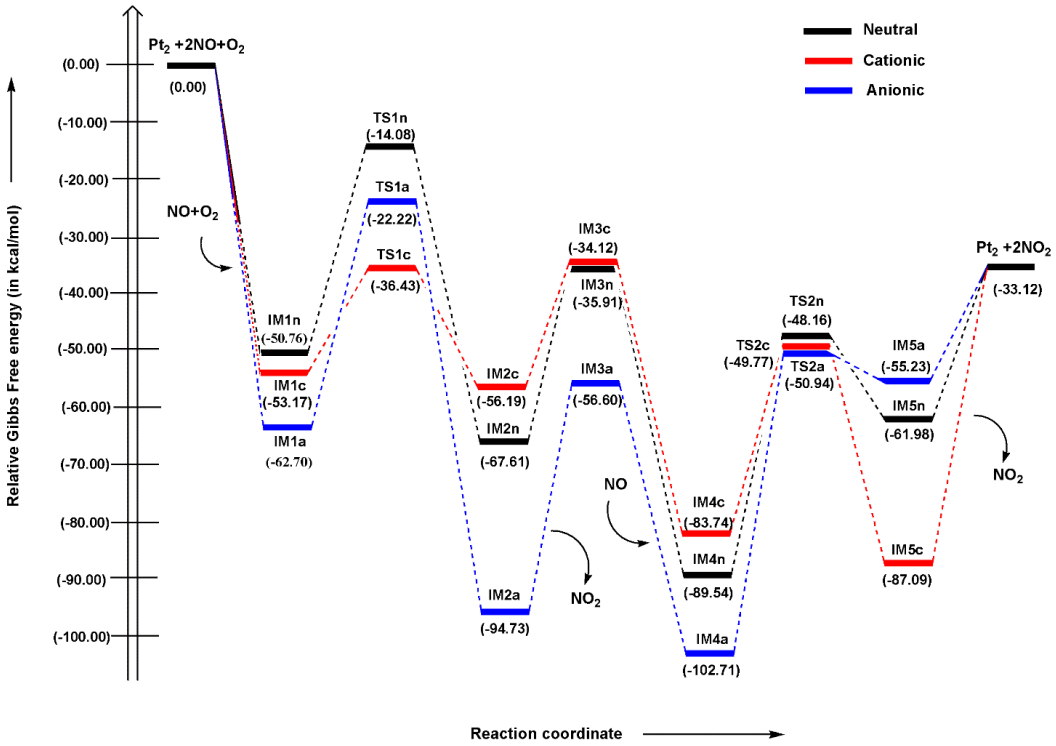

Figure 3.6: Calculated energy profile for LH-1 mechanism on $[Pt_2]^{0,\pm}$ dimers at M06L/def2TZVP level.

Optimized geometries of intermediates and transition states involved in catalytic oxidation pathway of NO via LH-2 on $[Pt_2]^0$, $[Pt_2]^+$, and $[Pt_2]^-$ dimers along with their bond lengths (in Å) are shown in Figure 3.7(a), (b) and (c). The relative energy profile diagram for the LH-2 mechanism has also been shown in Figure 8. In LH-2, the reaction mechanism starts with the co-adsorption of NO and O_2 on the same Pt atom present in the dimer. NO and O_2 are co-adsorbed on one of the Pt atoms of the neutral dimer, forming IM6n. Whereas co-adsorption of NO and O_2 on same Pt of $[Pt_2]^+$ and $[Pt_2]^-$ dimers results in the formation of IM6c and IM6a, respectively. In IM6n, after adsorption, O-O bond length is activated which is evident from its increased bond length (1.389 Å). Reaction advances via TS3n where one O atom of O_2 molecule interacts with the nearby N atom of NO molecule. In TS3n, the newly bond formed between N atom of NO and O atom of O_2 is about 1.534 Å which indicates interaction among them. TS3n is characterized by its only imaginary frequency (353.09***i*** cm^{-1}) and it is validated using IRC calculation where TS is showing smooth connectivity between its two nearby intermediates (IM6n and IM7n). In case of IM6c, N-O and O-O bond lengths are 1.127 Å and 1.214 Å, respectively which indicates little or no activation in both the reactants after the adsorption. It specifies minute or no transfer of electrons from Pt atoms to the antibonding orbitals of NO or O_2. Reaction proceeds via TS3c where elongation of O-O bond (1.215Å to 1.372Å) and formation of new N-O bond (1.466 Å) takes place. TS3c is validated by its only imaginary frequency (485.97***i*** cm^{-1}). Going forward, O-N-O-O bond structure is fully formed in IM7c which can be validated looking at the N-O and O-O bond lengths (1.339 Å and 1.451 Å, respectively). For $[Pt_2]^-$ dimer, intermediate IM6a has adsorbed N-O and O-O bond lengths of 1.184 Å and 1.296 Å, respectively, which indicates activation of both the reactants which aids in the reaction to proceed. TS3a occurs (imaginary frequency of 346.44***i*** cm^{-1}) where NO and O_2 interacts with each other to form O-N-O-O bond. Elongation of O-O bond (1.384 Å) and strengthening of N-O bond (1.593 Å) occurs in TS3a. From energy profile diagram, it is found that the activation barrier for TS3n, TS3c and TS3a are 35.40, 31.71 and 14.47 kcal/mol, respectively. It may be attributed to the fact that both NO and O_2 are well activated in IM6a which helps in reaction to proceed smoothly. The formation of O-N-O-O bond (TS1) is endothermic in all the dimers. Reaction proceeds via TS4n where scissoring of O-O bond takes place resulting in

the formation of first NO_2. In TS4n, the bond length of O-O bond increases from 1.457 Å to 1.780Å (shown in Figure 3.7) which indicates breaking of O-O bond. Again the TS is confirmed by its one imaginary frequency (633.53***i*** cm^{-1}). The activation barrier for this step is very low, i.e 6.57 kcal/mol. IM8n is formed in which first NO_2 is formed and removed subsequently, resulting in the formation of Pt_2-O species (IM3n). Same mechanism is followed in the cationic TS4c and anionic TS4a in which cleavage of O-O bond and formation of first NO_2 takes place. The barrier height for TS4c and TS4a are 6.35 kcal/mol and 6.22 kcal/mol. This step is feasible, both kinetically and thermodynamically, in all the three dimers. Incoming of another NO into the same site of Pt atom made adsorption mode of 'O' atom goes from linear to bridged manner in IM9n, IM9c and IM9a in the neutral, cationic and anionic species, respectively. Adsorption of NO molecule onto Pt_2-O species (IM3n, IM3c and IM3a) results in the formation of much stable intermediates IM9n, IM9c and IM9a which are 67.54 kcal/mol, 77.87 kcal/mol and 64.28 kcal/mol lower in energy than IM3n, IM3c and IM3a, respectively. It is attributed to the fact that both NO molecule and 'O' atom are strongly co-adsorbed into the $[Pt_2]^{0,\pm}$ dimers which made IM9 intermediate very much stable in PES. As a result, the formation of second NO_2 via TS5n, TS5c and TS5a is difficult, owning to their high activation barrier. The barrier height for the formation of second NO_2 via TS5n, TS5c and TS5a are 65.15 kcal/mol, 68.65 kcal/mol and 76.92 kcal/mol, respectively. The third step is highly endothermic in all the three dimers as depicted from Figure 3.8. Hence, the formation of second NO_2 is unfeasible (both kinetically as well as thermodynamically) via LH-2 mechanism in $[Pt_2]^{0,\pm}$ dimers. It is to note that the spin is conserved throughout the whole reaction. In $[Pt_2]^0$ dimer, whole reaction pathway undergoes via SM=2 whereas in both the cationic and anionic dimer, mechanism undergoes via SM=1.

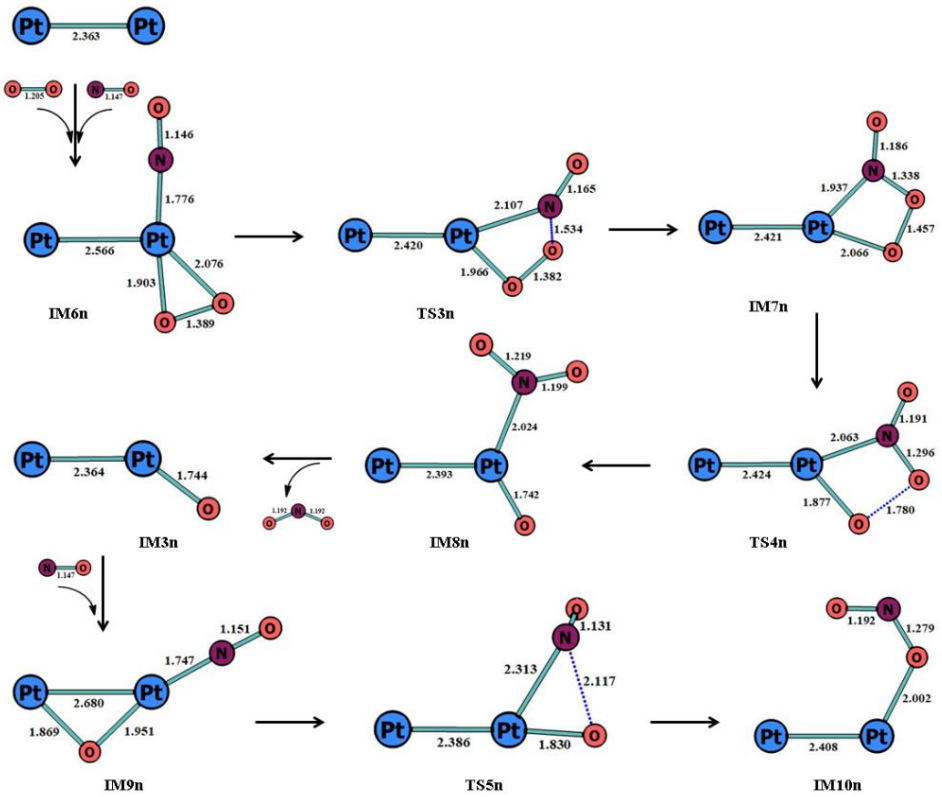
Pt
2.363
1.205
1.147
1.146
1.776
2.566
2.076
1.903
1.389
IM6n
2.107
1.165
1.534
2.420
1.966
1.382
TS3n
1.186
1.338
1.937
1.457
2.421
2.066
IM7n
1.219
1.199
2.024
2.393
1.742
IM8n
1.191
2.063
1.296
2.424
1.877
1.780
TS4n
2.364
1.744
IM3n
1.151
1.747
2.680
1.869
1.951
IM9n
1.131
2.313
2.117
2.386
1.830
TS5n
1.192
1.279
2.002
2.408
IM10n

(a)

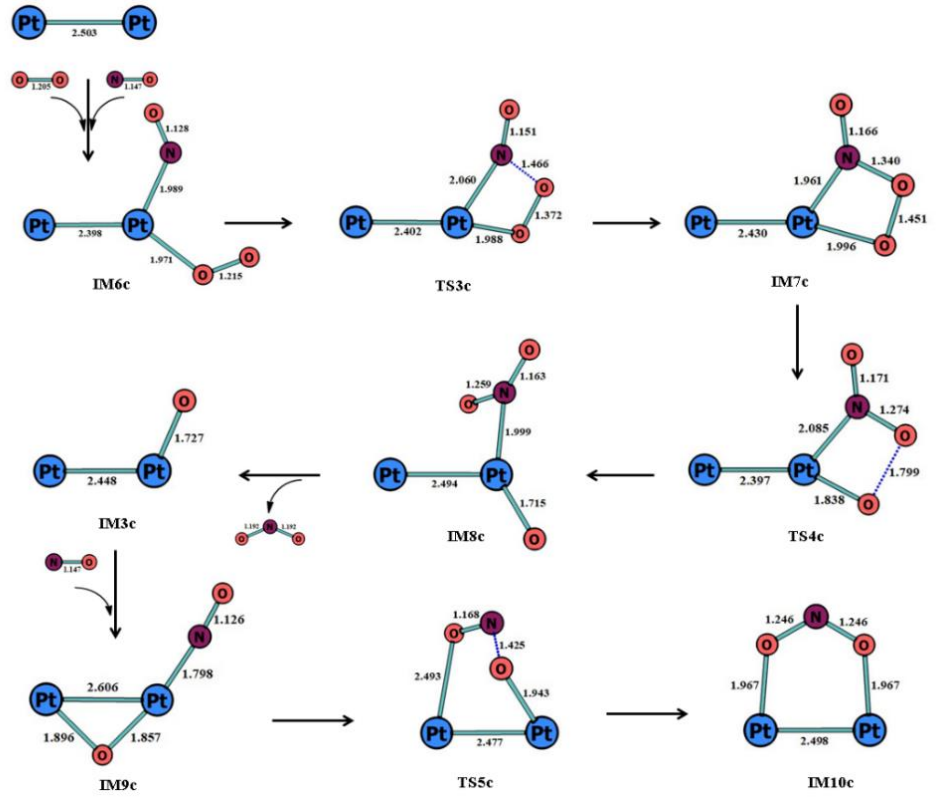
Pt
2.503
1.205
1.147
1.128
1.989
2.398
1.971
1.215
IM6c
1.151
1.466
2.060
1.372
2.402
1.988
TS3c
1.166
1.340
1.961
1.451
2.430
1.996
IM7c
1.727
2.448
IM3c
1.259
1.163
1.999
2.494
1.715
IM8c
1.171
1.274
2.085
1.799
2.397
1.838
TS4c
1.126
1.798
2.606
1.896
1.857
IM9c
1.168
1.425
2.493
1.943
2.477
TS5c
1.246
1.246
1.967
1.967
2.498
IM10c

(b)

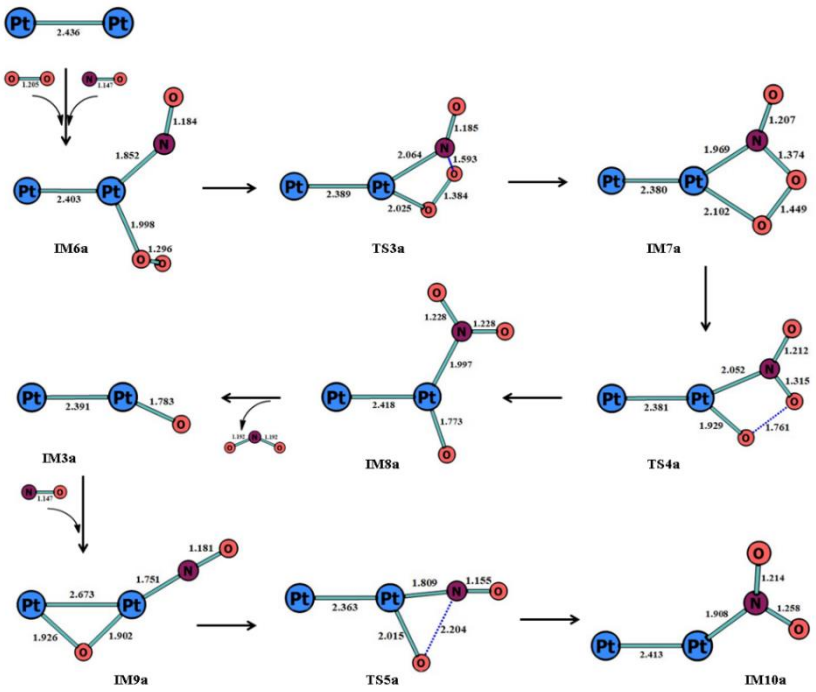

(c)

Figure 3.7: Optimized geometries of intermediates and transition states involved in catalytic oxidation pathway of NO via LH-2 mechanism on (a) $[Pt_2]^0$ dimer (b) $[Pt_2]^+$ dimer and (c) $[Pt_2]^-$ dimer along with their bond lengths (in Å).

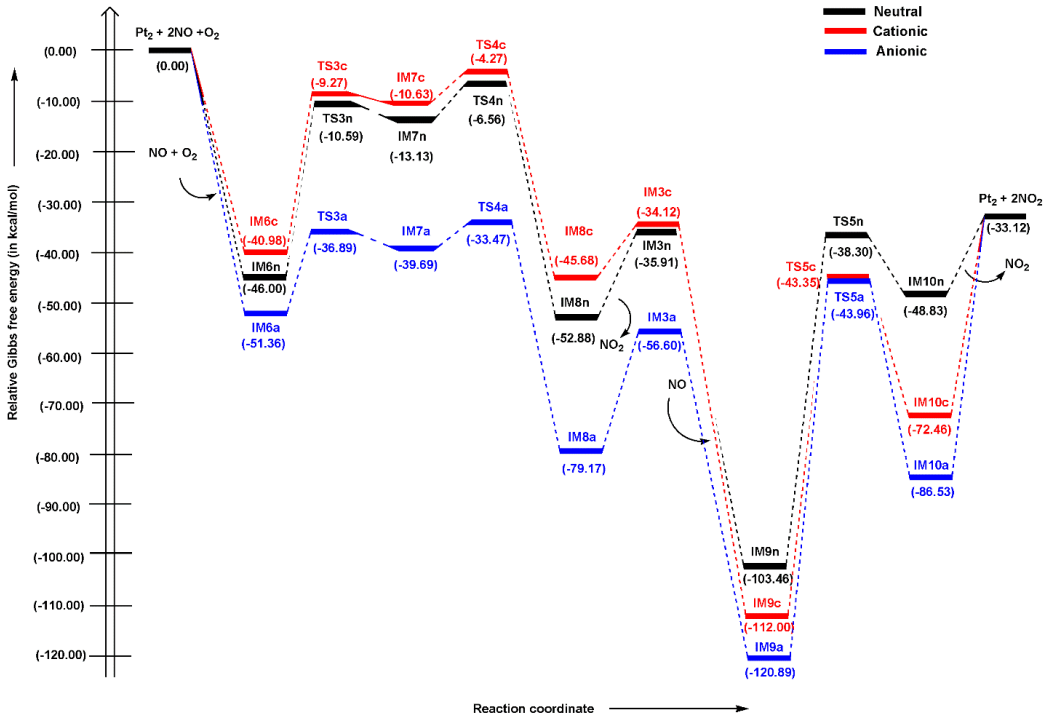

Figure 3.8: Calculated energy profile for LH-2 mechanism on $[Pt_2]^{0,\pm}$ dimers at M06L/def2TZVP level.

Table 3.9 contains calculated barrier heights (in kcal/mol) for mechanism LH-1 and LH-2 on $[Pt_2]^{0,\pm}$ dimers at M06L/def2TZVP level. Looking at the activation barrier, it can be concluded that LH-1 mechanism is possible on cationic Pt_2 dimers. For LH-2 mechanism, TS1 and TS2 represents the formation of first NO_2 while TS3 represents the formation of second NO_2. $[Pt_2]^-$ dimer possesses lowest energy barrier for TS1 and TS2 as compared to its other counterparts. Hence, the formation of first NO_2 is highly feasible in anionic $[Pt_2]^-$ dimer. However, the formation of second NO_2 is highly unlikely as TS3 possesses high activation barrier for all the three systems. It is important to note that both the NO molecules are converted to NO_2 in LH-1 mechanism in cationic Pt dimer.

Table 3.9: Calculated barrier heights (in kcal/mol) for LH-1 and LH-2 on $[Pt_2]^{0,\pm}$ dimers at M06L/def2TZVP level.

Catalyst	LH-1		LH-2		
	TS1	TS2	TS1	TS2	TS3
$[Pt_2]^0$	36.67	41.37	35.40	6.57	65.15
$[Pt_2]^+$	16.74	33.96	31.71	6.35	68.65
$[Pt_2]^-$	40.48	51.76	14.47	6.22	76.92

3.3.3.2 Termolecular Eley Rideal (TER) mechanism

The TER mechanism is a three molecular reaction mechanism in which the gaseous O_2 molecule is activated by two pre-adsorbed NO molecules. As previously discussed, the co-adsorption of two NO molecules on $[Pt_2]^{0,\pm}$ dimers is stronger than co-adsorption of NO and O_2 as well as single adsorption of NO and O_2. Hence, NO oxidation may also proceed via TER mechanism. The initial co-adsorption of two NO molecules may take place at nearby Pt atoms or at the same location on a single Pt atom, resulting in two distinct reaction pathways, designated TER-1 and TER-2, respectively. Figure 3.9 (a) and (b) demonstrate, respectively, the optimized geometries of intermediates and transition states involved in the catalytic oxidation pathway of NO via TER-1 and TER-2 on $[Pt_2]^0$ dimers.

The reaction mechanism starts with the co-adsorption of two NO molecules on the alternative Pt atoms of neutral dimers, forming IM11/n. This intermediate is

80.05 kcal/mol stable in energy than the starting material (Pt_2 + 2NO + O_2). Inclusion of O_2 molecule leads to the formation of IM12/n which becomes lower in energy (by 22.22 kcal/mol) than that of IM11/n. In IM12/n, as evident from the bond distance, O_2 has negligible interaction with that of Pt atoms or NO molecules. The O-O bond length and $\upsilon_{O\text{-}O}$ in IM12/n is 1.208 Å and 1608.09 cm^{-1}, respectively which indicates minimum or no activation of O_2 at all. Reaction proceeds via TS6/n where O_2 interacts with two NO molecules adsorbed adjacently to the Pt atoms. Elongation of O-O bond length (1.561 Å) and formation of two new N-O bonds (1.420 Å and 1.422 Å) takes place. This TS is confirmed by its imaginary frequency 827.46***i*** cm^{-1} and the barrier height for this step is 89.87 kcal/mol. Hence, the reaction mechanism is not favourable as the transition barrier is too high. The large barrier height is attributed to the fact that O_2 was not activated at all in IM12/n. Additionally, the considerable distance between two NO molecules makes it challenging for O_2 to react with both of them simultaneously.

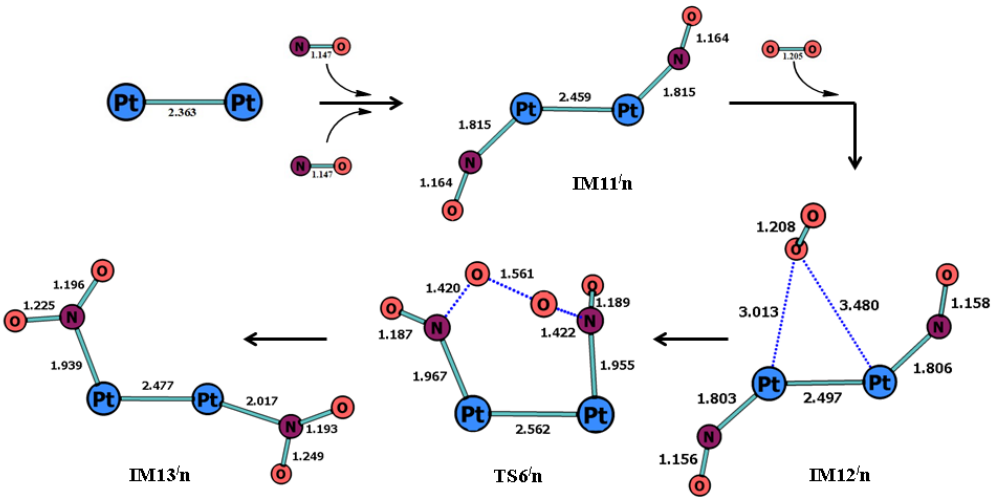

(a)

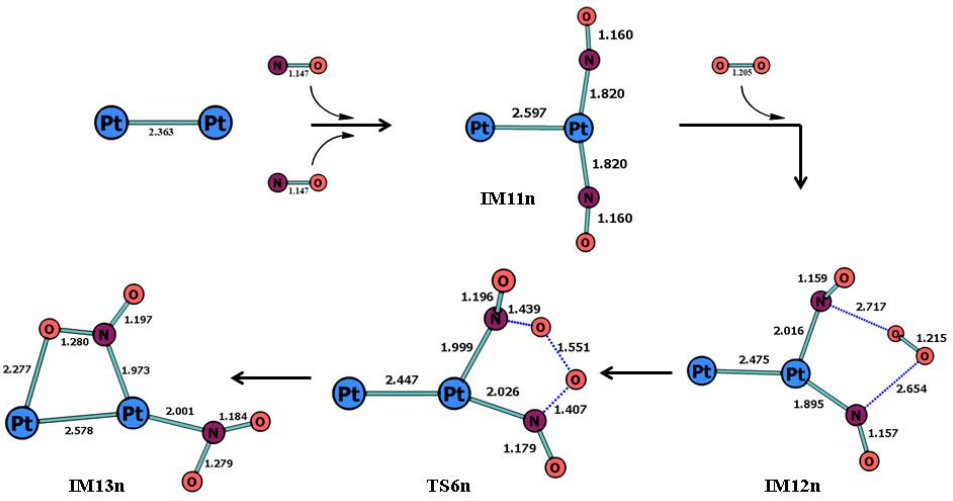

(b)

Figure 3.9: Optimized geometries of intermediates and transition states involved in catalytic oxidation pathway of NO on $[Pt_2]^0$ dimer via (a) TER-1 and (b) TER-2 along with their bond lengths (in Å).

TER-2 starts with the co-adsorption of two NO molecules on the same Pt site of $[Pt_2]^0$ dimer forming IM11n, which is 70.05 kcal/mol lower in energy than the starting point. One O_2 molecule approaches the two NO molecules while remaining at gas phase. The bond distances between two NO and O_2 molecule are 2.654 Å and 2.717 Å. In IM12n, O_2 molecule is slightly activated ($d_{O\text{-}O}$=1.215Å; $\upsilon_{O\text{-}O}$=1526.85 cm^{-1}) as compared to its free form ($d_{O\text{-}O}$=1.205 Å; $\upsilon_{O\text{-}O}$=1645.64 cm^{-1}). Reaction goes forward when two oxygen atoms binds to the N atoms of two NO molecules (TS6n). O-O bond is cleaved and two new N-O bonds are formed in TS6n. The activation energy for this step is 45.53 kcal/mol. In IM13n, two NO_2 molecules are fully formed and attached to the neutral dimer, which is 81.68 kcal/mol energy lower than the starting point. This step is exothermic by 28.82 kcal/mol and the desorption energy of two NO_2 molecules from the neutral system is 48.55 kcal/mol.

For $[Pt_2]^+$ and $[Pt_2]^-$ dimer, reaction mechanism TER-1 doesn't occur as O_2 gets adsorbed to $[Pt_2]^{\pm}$ dimers owing to the greater distance between two NO molecules due to their adsorption on adjacent Pt atoms. However, TER-2 mechanism is followed by both the cationic and anionic systems. For $[Pt_2]^+$ dimer, IM11c is formed when two NO molecules are adsorbed on the same site. The intermediate is 83.38 kcal/mol lower in energy w.r.t starting point in PES. O_2 molecule enters the system, interacting with two NO molecules from a distance, forming IM12c. Looking at the

bond distance (1.203 Å) and vibrational frequency (1640.16 cm^{-1}), there is no activation of O_2 occurring in IM12c. Reaction proceeds via TS6c where O_2 interacts with two NO molecules forming O-N-O-O-N-O bond. TS is characterized by its imaginary frequency 1007.36***i*** cm^{-1} and the barrier height is 62.69 kcal/mol. The barrier height is very high as a lot of energy is required to activate the inactivated O_2. IM13c is formed where two NO_2 molecules are attached to the same Pt atom. IM13c is 57.77 kcal/mol lower in energy than that of TS6c. Figure 3.10 contains optimized geometries of intermediates and transition states involved in catalytic oxidation pathway of NO on $[Pt_2]^+$ dimer via TER-2.

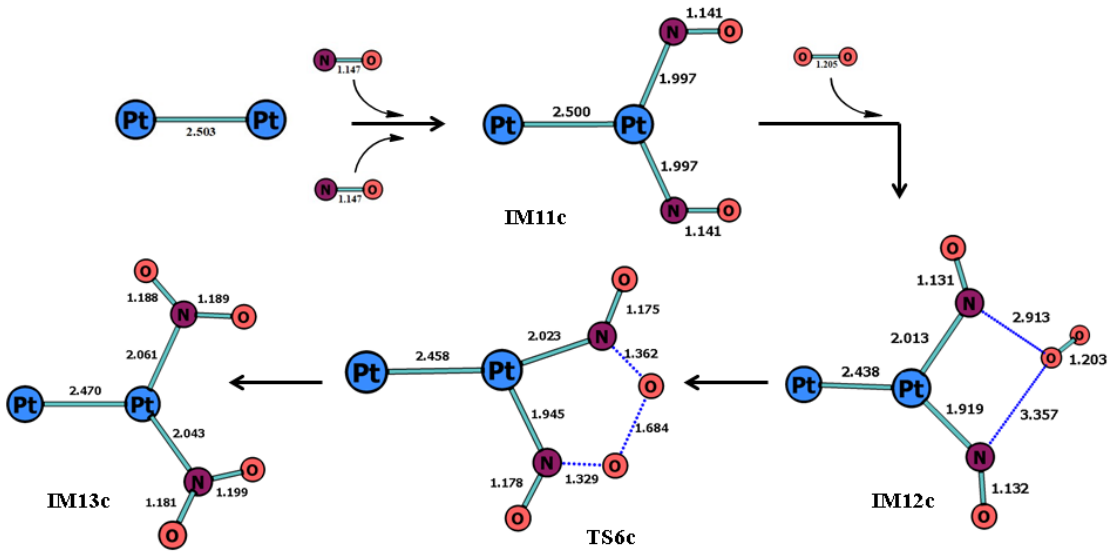

Figure 3.10: Optimized geometries of intermediates and transition states involved in catalytic oxidation pathway of NO on $[Pt_2]^+$ dimer via TER-2 along with their bond lengths (in Å).

Figure 3.11 (a) and (b) contains IMs and TSs involved in NO oxidation on $[Pt_2]^-$ dimer via TER-2 and TER-3, respectively. TER-2 undergoes via one TS where two oxygen atoms of O_2 binds to the N atoms of NO molecules and cleave itself in one step, forming two NO_2. TER-3 exhibits similarities to TER-2 in that both mechanisms occur in a singular Pt site. In the context of TER-3, the reaction mechanism involves the participation of two transition states (TS). The initial step entails the contact between an O_2 molecule and one NO, while the subsequent step involves the breaking of the O-O bond due to its interaction with the second NO.

IM11a is formed after adsorption of two NO molecules on $[Pt_2]^-$ dimer, 66.83 kcal/mol lower in energy than the initial point. Addition of O_2 on IM11a results in

the formation of IM12a, which is lower in energy than that of IM11a (by 5.69 kcal/mol). O_2 remains in the gas phase while interacting with two NO molecules from a distance (3.089 Å and 3.419Å). Slight activation of O_2 takes place in IM12a as evident from its bond length (1.223 Å) and frequency (1467.92cm^{-1}). Reaction make progress via TS6a (862.44***i*** cm^{-1}) where O-O bond breaks while interacting with two NO molecules. The activation barrier going from IM12a to TS6a is 49.43 kcal/mol. At last, IM13a is formed where two NO_2 molecules are formed. Whole reaction mechanism proceeds in quartet spin state (SM=4).

TER-3 starts with the co-adsorption of two NO molecules on $[Pt_2]^-$ dimer, forming IM11/a in doublet spin state (SM=2). Further inclusion of O_2 results in the formation of IM12/a. TS6/a is formed when O_2 molecule reacts with one of the NO molecule with an imaginary frequency, 481.39***i*** cm^{-1}. Bond parameters clearly show elongation of O-O bond (from 1.240 Å to 1.306 Å) and strengthening of N-O bond (2.505 Å to 1.549 Å). IM13/a is formed after TS6/a where O-N-O-O bond is present. The first step is endothermic by 17.44 kcal/mol. In TS7/a, O-O bond breaking takes place (from 1.334 Å to 1.597Å) while interacting with second NO, thus forming O-N-O-O-N-O species. This resulted in the formation of two NO_2 molecules in IM14/a. The second step of TER-3 is highly exothermic (58.19 kcal/mol). Hence, our second step is the driving force for the reaction to occur. The barrier height for TS6/a and TS7/a are 17.42 kcal/mol and 20.18 kcal/mol, respectively. The energies of the two NO_2 molecules to get desorbed from the anionic system is 81.81 kcal/mol. Figure 3.12 contains PES for TER-1, TER-2 and TER-3 mechanisms on $[Pt_2]^{0,\pm}$ dimers at M06L/def2TZVP level.

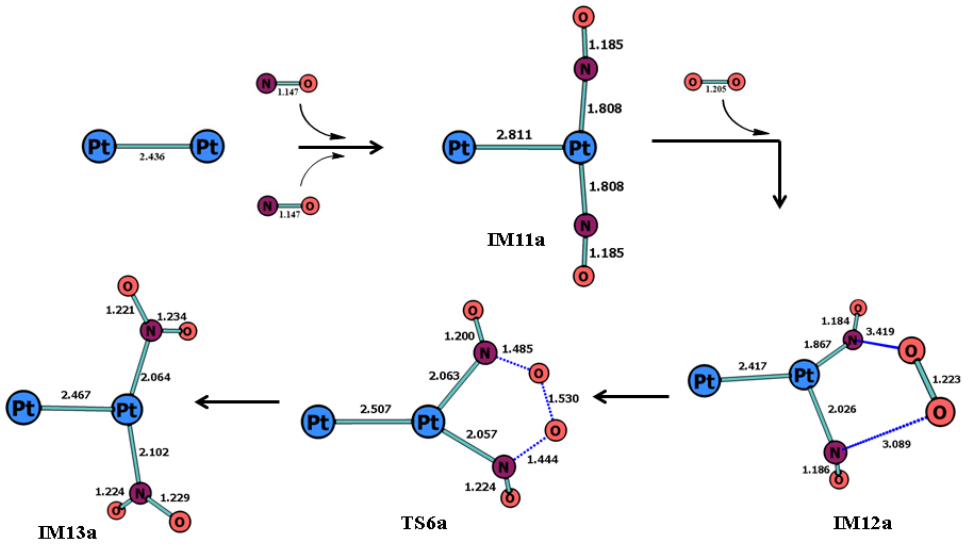

(a)

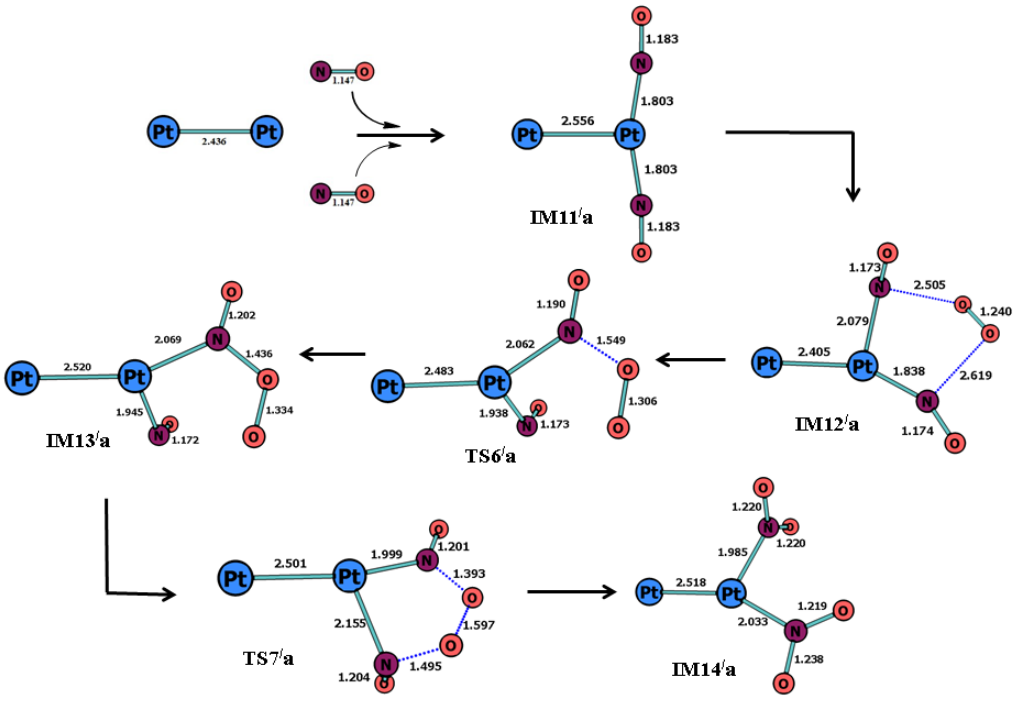

(b)

Figure 3.11: Optimized geometries of intermediates and transition states involved in catalytic oxidation pathway of NO on $[Pt_2]^-$ dimer via (a) TER-2 (b) TER-3 along with their bond lengths (in Å).

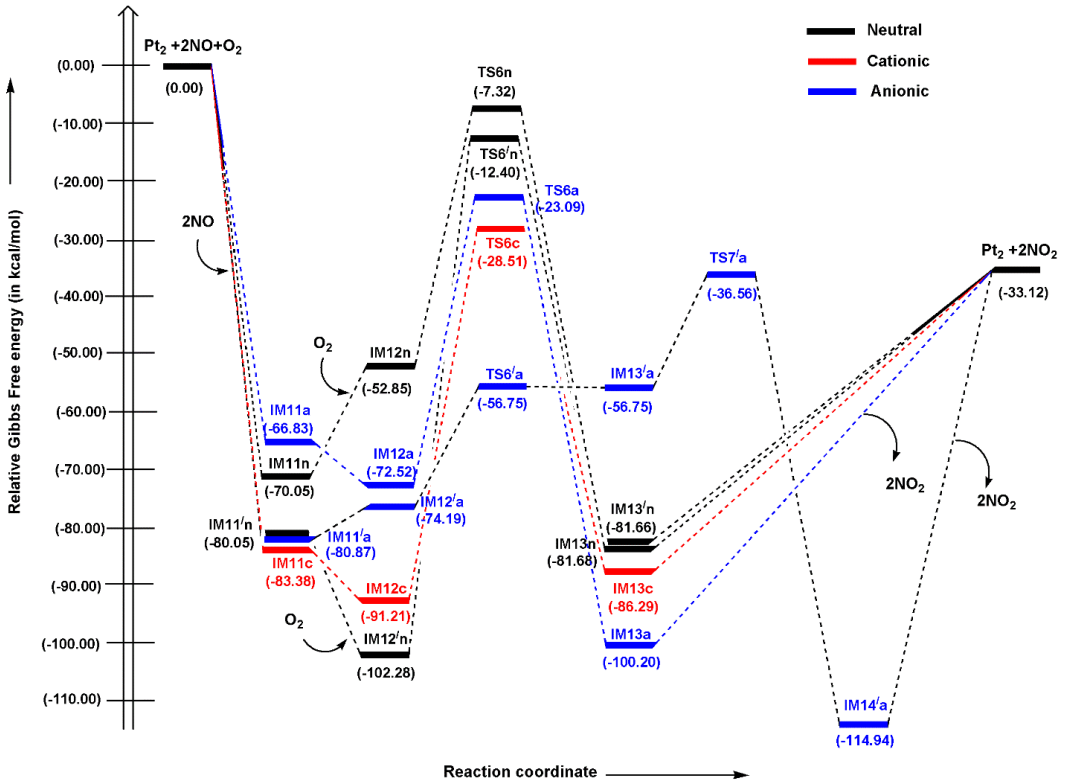

Figure 3.12: Calculated energy profile for TER-1, TER-2 and TER-3 mechanisms on $[Pt_2]^{0,\pm}$ dimers at M06L/def2TZVP level.

Table 3.10 contains activation barrier (in kcal/mol) for TER-1, TER-2 and TER-3 on $[Pt_2]^{0,\pm}$ dimers at M06L/def2TZVP level. As we can see, the TER-2 mechanism is followed in all the three dimers because the mechanism involves only one site, making it simpler for two NO molecules to engage with the O_2 molecule and retaining it in the gaseous phase (which is important for an Eley-Rideal mechanism). However, when it comes to more than one site (TER-1), the distance between two NO molecules increases, thus, making it difficult for them to contain O_2 in gas phase. TER-1 is only followed on $[Pt_2]^0$ dimer as the individual O_2 adsorption on neutral dimer is low (-19.79 kcal/mol). However, due to the high individual O_2 adsorption on cationic and anionic dimers (-48.65 kcal/mol and -42.76 kcal/mol, respectively), it is challenging for two NO molecules to contain O_2 in the gas phase since O_2's natural tendency is to interact with the Pt atom. TER-3 is a special mechanism which undergoes via two transition states and is seen in case of anionic Pt dimer. A critical step in the TER mechanism is the activation of O_2 by its interaction with two NO molecules. Due to the large distance between two NO molecules and O_2, it is difficult for NO molecules to interact with O_2 and activate it,

making the activation barrier of TER-1 very high (89.87 kcal/mol). Bond parameters of O_2 in IM12/n confirms the inactivated state of O_2 (d_{O-O}=1.208Å; υ_{O-O}=1608.09 cm^{-1}). Same is the case for TER-2 in all the three dimers where O_2 is barely activated in their respective intermediates (IM12n, IM12c and IM12a). Table 3.11 includes bond parameters (d_{O-O} bond length and υ_{O-O} vibrational frequency) of intermediates IM12 (n, c and a) of different dimers for TER-1, TER-2 and TER-3. It is clear from Table 3.11 that the activation of O_2 is maximum in case of TER-3 for $[Pt_2]^-$ dimers, which directly influences the activation barrier (Table 3.10). Hence, from Table 3.10 and Table 3.11, we conclude that TER-3 mechanism is feasible for catalytic oxidation of NO to NO_2 on $[Pt_2]^-$ dimer while TER-1 and TER-2 are energetically not favourable.

Table 3.10: Calculated barrier heights (in kcal/mol) for TER-1, TER-2 and TER-3 on $[Pt_2]^{0,\pm}$ dimers at M06L/def2TZVP level.

Catalyst	Activation barrier (in kcal/mol)			
	TER-1	TER-2	TER-3	
	TS6/	TS6	TS6/	TS7/
$[Pt_2]^0$	89.87	45.53	---	---
$[Pt_2]^+$	---	62.69	---	---
$[Pt_2]^-$	---	49.43	17.42	20.18

Table 3.11: Calculated bond distance (d_{O-O} (in Å)) and frequencies (υ_{O-O} (in cm^{-1})) of O_2 molecule present in intermediate IM12 (n, c and a) for TER-1, TER-2 and TER-3 on $[Pt_2]^{0,\pm}$ dimers at M06L/def2TZVP level.

Catalyst	TER-1		TER-2		TER-3	
	d_{O-O}(in Å)	υ_{O-O} (in cm^{-1})	d_{O-O}(in Å)	υ_{O-O}(in cm^{-1})	d_{O-O}(in Å)	υ_{O-O}(in cm^{-1})
$[Pt_2]^0$	1.208	1608.09	1.215	1526.85	---	---
$[Pt_2]^+$	---	---	1.203	1640.16	---	---
$[Pt_2]^-$	---	---	1.223	1467.92	1.240	1393.23

3.3.3.3 Termolecular Langmuir Hinshelwood (TLH) mechanism

Termolecular Langmuir Hinshelwood (TLH) mechanism is another three-molecule reaction mechanism in which two NO molecules and one O_2 molecule, all are co-adsorbed onto the catalyst to interact with each other. TLH mechanism has been followed in all the three dimers.

The co-adsorption of two NO molecules onto the same Pt atom in neutral dimers initiate the process, resulting in the formation of IM14n. One NO molecule in IM14n is adsorbed in a linear fashion, whereas the other is adsorbed in a bridged manner, with the NO atoms' N and O bound to the nearby Pt atoms. Energy-wise, this intermediate is 53.61 kcal/mol more stable than the starting point. Inclusion of O_2 molecule leads to the gain in energy leading to the formation of IM15n (39.32 kcal/mol in PES). It can be observed in IM15n that the O_2 molecule is sufficiently activated to advance the reaction. The bond length of O_2 (1.255 Å) and $\upsilon_{O\text{-}O}$ (1269.69 cm^{-1}) in IM15n also reflects the same. Reaction proceeds via TS7n (imaginary frequency=141.51***i*** cm^{-1}) where O atom of O_2 interacts with the bridging N atom of NO molecule, forming IM16n. This step is exothermic by 6.12 kcal/mol and the activation barrier is 3.34 kcal/mol. Hence, this step is both kinetically and thermodynamically feasible. In the second TS, the second O atom of O_2 interacts with the other linear NO molecule, making a cyclic O-N-O-O-N-O species. The activation barrier for this step is 37.75 kcal/mol and the step is highly exothermic by 58.15 kcal/mol. IM17n is formed way below the starting point (-103.61 kcal/mol), indicating the high stability of the intermediate. The desorption energy for both the NO_2 molecules are 70.48 kcal/mol (35.24 kcal/mol for each NO_2).

In cationic species, two NO molecules are adsorbed in the similar manner as that of neutral species, forming IM14c. Interaction of O_2 with IM14c leads to the formation of IM15c. IM14c and IM15c are -97.41 kcal/mol and -94.53 kcal/mol in Potential Energy Surface, respectively. TLH in $[Pt_2]^+$ undergoes via one TS where one O_2 interacts with two NO molecules simultaneously to form two NO_2 molecules. The barrier height for this step is 68.29 kcal/mol, which indicates that the reaction is not possible. This huge barrier is due to the fact that O_2 is not at all activated in IM15c where $d_{O\text{-}O}$ is 1.203 Å and $\upsilon_{O\text{-}O}$ is 1613.96 cm^{-1}. IM16c is formed where two NO_2 molecules are formed and bonded to the cationic dimer catalyst.

In $[Pt_2]^-$ dimer, one NO is bonded in a linear fashion whereas the other NO is bonded in a bridging manner where N atom is attached to both the Pt atoms (IM14a). Reaction is carried forward by inclusion of O_2 in IM14a, forming IM15a. IM14a and IM15a are positioned very low in PES, i.e. -101.61 kcal/mol and -94.64 kcal/mol, respectively. TS7a results in the interaction of O_2 with the linear NO to form IM16a. The barrier height for this step is 11.63 kcal/mol and the TS is characterized by its imaginary frequency, 275.58***i*** cm^{-1}. This step is endothermic by 7.95 kcal/mol. Elongation of O-O bond (1.430 Å in IM16a to 1.707 Å in TS8a) takes place in TS8a where the bond gets broken, giving rise to IM17a. The TS8a has one imaginary frequency of 1231.39***i*** cm^{-1} and the barrier height is 8.72 kcal/mol. This step is thermodynamically feasible as it is highly exothermic (by 27.82 kcal/mol). First NO_2 molecule gets release from the system at a very low desorption energy of 2.61 kcal/mol. After releasing of first NO_2, the mechanism goes from being trimolecular to bimolecular reaction. Reaction is carried forward via TS9a where single 'O' atom interacts with the bridged NO molecule with a huge activation barrier of 81.46 kcal/mol. Hence, the formation of second NO_2 is not feasible in anionic system via TLH mechanism. Figure 3.13 (a), (b) and (c) contains IMs and TSs involved in NO oxidation on $[Pt_2]^0$ $[Pt_2]^+$ and $[Pt_2]^-$, respectively via TLH. Figure 3.14 contains PES for TLH mechanism on $[Pt_2]^{0,\pm}$ dimers at M06L/def2TZVP level. It is worth noting that for all the reaction mechanism performed above, spin is conserved during the whole pathway.

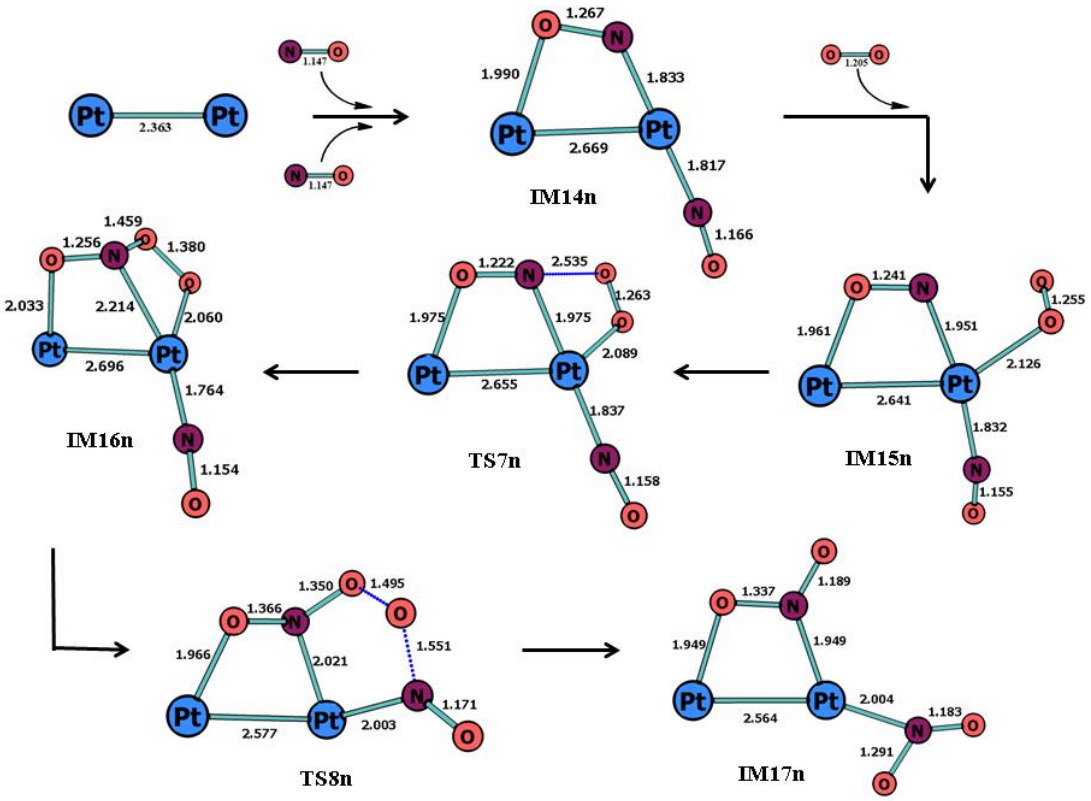

(a)

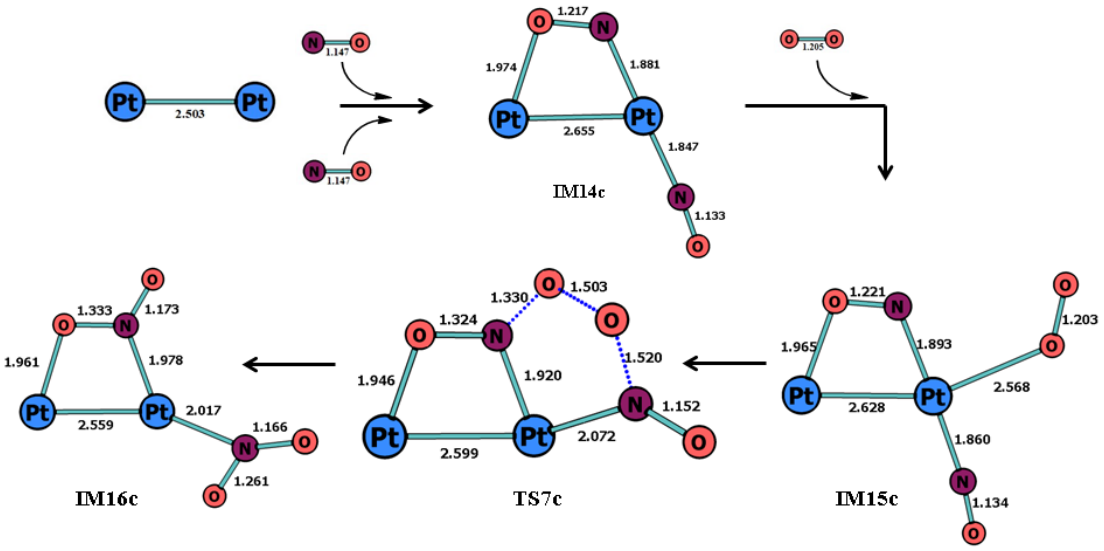

(b)

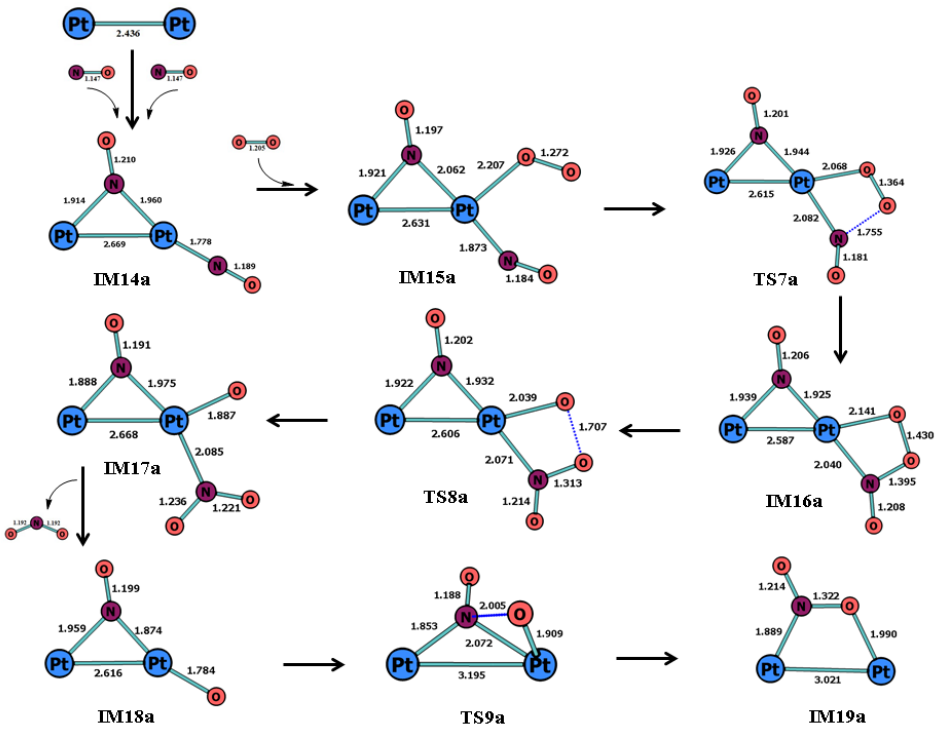

(c)

Figure 3.13: Optimized geometries of intermediates and transition states involved in catalytic oxidation pathway of NO on (a) $[Pt_2]^0$ (b) $[Pt_2]^+$ and (c) $[Pt_2]^-$ dimer via TLH along with their bond lengths (in Å).

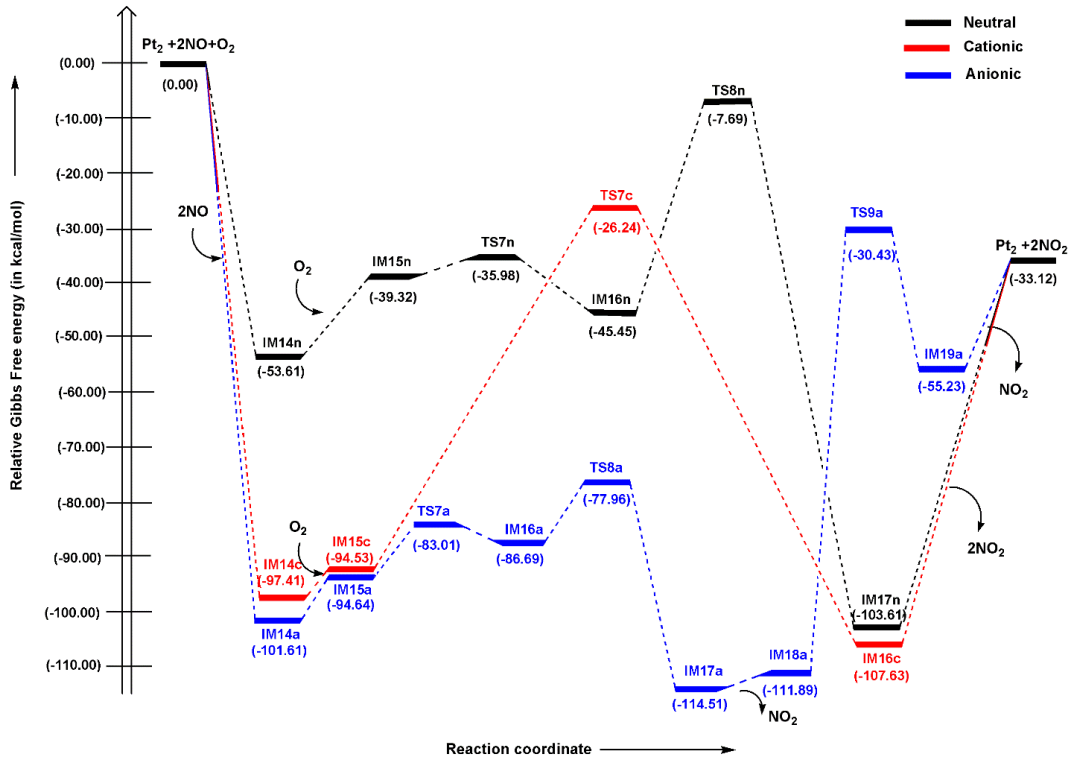

Figure 3.14: Calculated energy profile for TLH mechanism on $[Pt_2]^{0,\pm}$ dimers at M06L/def2TZVP level.

Table 3.12 contains activation barrier (in kcal/mol) for TLH on $[Pt_2]^{0,\pm}$ dimers at M06L/def2TZVP level. Two NO_2 molecules are removed simultaneously from a neutral and cationic dimer, whereas in an anionic system, two NO_2 molecules are removed in a step by step process. $[Pt_2]^0$ dimer consists of two TSs (TS7n and TS8n) for the formation of two NO_2 molecule. The activation barrier for TS7n and TS8n are 3.34 and 37.75 kcal/mol, respectively. Hence, the formation of two NO_2 is possible for neutral dimer. For $[Pt_2]^+$ dimer, the activation barrier of TS7c is 68.29 kcal/mol which suggests that TLH mechanism will not be followed by cationic dimer. In anionic system, the formation of first NO_2 molecule occurs via TS7a and TS8a, with barrier heights of 11.63 and 8.72 kcal/mol, respectively while the formation of second NO_2 molecule occurs via TS9a, with a barrier height of 81.46 kcal/mol. Hence, we conclude that the formation of first NO_2 molecule is feasible; however, the formation of second NO_2 is not feasible.

Table 3.12: Calculated barrier heights (in kcal/mol) for TLH on $[Pt_2]^{0,\pm}$ dimers at M06L/def2TZVP level.

Catalyst	Activation barrier (in kcal/mol)		
	TLH		
	TS7	**TS8**	**TS9**
$[Pt_2]^0$	3.34	37.75	---
$[Pt_2]^+$	68.29	---	---
$[Pt_2]^-$	11.63	8.72	81.46

Comparing the activation barrier of LH, TER and TLH mechanisms, we conclude that TER mechanism, particularly TER-3, is found to be most proficient mechanism for the conversion of 2 NO into 2 NO_2. More recently, single atom catalysts are found to be effective catalysts for NO oxidation and have been studied extensively [27, 59, 61, 66, 67]. Yang *et al.* [59] performed NO oxidation using single Fe atom with single vacancy graphene based substrate (Fe/SV) in which the range of activation barrier with six different paths is found to be 0.04 eV (0.92 kcal/mol) to 2.17 eV (50.04 kcal/mol). The most dominant path was found to be of E-R mechanism with energy barrier of 0.04 eV. However, they also established that the desorption process of NO_2 from the catalyst is found to be slow due to its higher

desorption energy. Although the energy barrier of our system is slightly higher with respect to Fe/SV but the desorption energy of two NO_2 molecules via our most efficient path (TER-3) is found to be lower (40.90 kcal/mol for each NO_2). Liu and his co-workers [66] have systematically studied NO oxidation on bimetallic site of (Fe, Co) supported on N-doped graphene in which the activation energy is found within the range of 0.17 -0.91 eV. They also observed L-H mechanism with desorption barrier of 1.52 eV to be the most proficient one. Tang *et al.* [27] performed NO and CO oxidation reactions on single Pt and Pd anchored at graphylene substrate in which they found that reaction occurrence possibility of TER mechanism is more owing to its smaller energy barriers.

DFT study for elementary step of NO oxidation on clean Pt (111) surface resulted in activation barrier in the range of. 28-30 kcal/mol [68]. However, reaction is highly dependent on O_2 coverage. Moreover, NO oxidation is done on single supported Pt atoms using modified Langmuir Hinshelwood mechanism where rate constants and TOF values were found to be in concurrence with our result [23]. However, very less literature is available for NO oxidation on large Pt clusters where extensive mechanistic investigation is provided. Overall, it can be concluded that our proposed catalyst works fairly well and easily comparable with other efficient systems.

3.3.3.4 Thermodynamic and Kinetic analysis

The temperature of fuel gas in coal fired power plants ranges from 298.15 K to 1000 K [60]. Here, reaction spontaneity and kinetics of the most dominant path, that is, termolecular EleyRideal (TER-3) mechanism for anionic dimer system has been studied under the above temperature range. Table 3.13 shows changes in reaction spontaneity under different reaction temperatures. Reaction spontaneity (ΔG) is the difference between sum of free energies of final product (catalyst + $2NO_2$) and sum of free energies of starting material (catalyst +2 NO +O_2). Using Table 3.13, the effect of different temperatures on reaction spontaneity is presented in Figure 3.15. From Figure 3.15, it is evident that the reaction energies for the NO oxidation increases as the reaction temperature increases, depicting that the increase in temperature has an inhibiting effect on the spontaneity of the reactions. Hence, NO

oxidation process is more feasible at room temperature and its spontaneity decreases as the temperature increases.

Table 3.13: Changes in reaction spontaneity (ΔG) within the temperature range of 298.15-1000 K.

ΔG	Temp.
-33.12	298.15
-29.83	400
-26.48	500
-23.11	600
-19.73	700
-16.34	800
-12.96	900
-9.59	1000

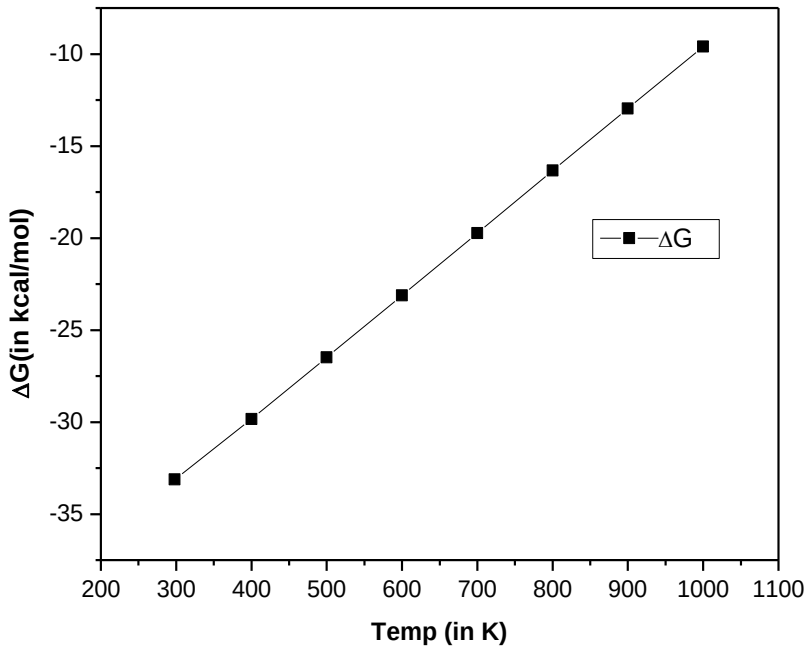

Figure 3.15: Changes in reaction spontaneity (ΔG) under different reaction temperatures (298.15-1000 K).

Desorption energies of two NO_2 molecules for TER-3 mechanism at different temperatures has also been studied and tabulated in Table 3.14. Table 3.14 suggests that desorption energies decrease as the temperature rises which means as the

temperature increases, it becomes easier for two NO_2 molecules to get desorbed from the catalytic dimer.

Table 3.14: Changes in desorption energies (ΔG_{des}) of two NO_2 molecules for TER-3 mechanism under different reaction temperatures.

Temp.	ΔG_{des} (in kcal/mol)
298.15	81.81
400	75.12
500	68.71
600	62.41
700	56.23
800	50.14
900	44.13
1000	38.20

The relative Gibbs free energy values are obtained from the TER-3 mechanism on $[Pt_2]^-$ dimer, when inserted in the Eq. 5 along with k_B, h, and T values in TST theory, the rate constant values are obtained. The calculated overall rate constants were fitted with the three parameters of the Arrhenius equation using the modified Arrhenius expression ($k = AT^n exp(-Ea/RT)$) within the temperature range of 298.15–1000 K and the modified expressions are given below as:

$$k_1 = 1.47 \times 10^{13} T^{(-1.06)} \exp(-7238.29 \pm 10.37)/T) \quad (11)$$

$$k_2 = 7.04 \times 10^{11} T^{(0.02)} \exp(-9550.38 \pm 5.29)/T) \quad (12)$$

where k_1 represents rate constant for the step corresponding to TS6/ and k_2 represents rate constant for the step corresponding to TS7/. We have performed custom fitting function in ORIGIN software [69] where the date (T vs k) was provided and non-linear fit was calculated. Table 3.15 represents rate coefficients (in s^{-1}) with respect to the temperature range of 298.15–1000 K for the TER-3 mechanism and Figure 3.16 describes changes in logarithm of reaction rate constants under different reaction temperatures for the same mechanism. It is evident from figure 3.16 that the rate constants are always increasing with the increase in temperature, which suggests that high temperature can speed up the catalytic oxidation of NO. Moreover, value of k_2 increases much more with increase

in temperature with respect to k_1. Hence, temperature has a promoting effect on the reaction rate of NO oxidation.

Table 3.15: Calculated rate coefficients (in s^{-1}) within the temperature range of 298.15–1000 K for the TER-3 mechanism at the M06L/def2TZVP level of theory.

Temp (in K)	k_1	k_2
298.15	9.96×10^{-1}	9.60×10^{-3}
400	3.56×10^{2}	3.38×10^{1}
500	1.04×10^{4}	4.01×10^{3}
600	9.57×10^{4}	9.70×10^{4}
700	4.55×10^{5}	9.44×10^{5}
800	1.44×10^{6}	5.21×10^{6}
900	3.48×10^{6}	1.97×10^{7}
1000	6.98×10^{6}	5.72×10^{7}

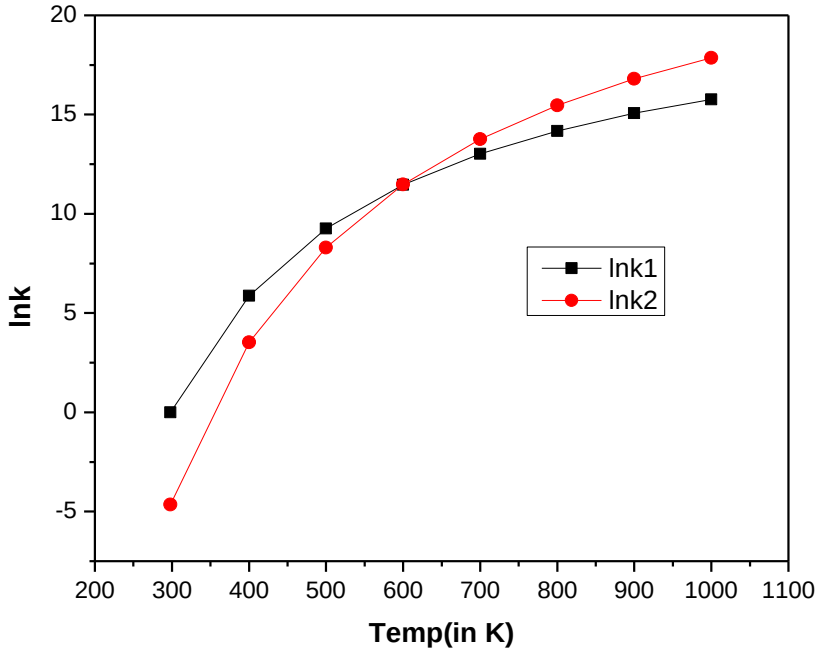

Figure 3.16: Changes in logarithm of reaction rate constants under different reaction temperatures for TER-3 mechanism.

3.4 Significant Outcomes

In summary, we have studied the catalytic oxidation of NO to NO_2 on $[Pt_2]^{0,\pm}$ dimers using M06L/def2TZVP level of theory. 15 different functionals with density-fitting triple-ζ valence single polarization (def2TZVP) basis set is tested, in which values given by the M06L functional are found to be in close proximity to the experimental ones.

1. Electronic structure calculations suggest the $[Pt_2]^-$ dimer to be the most chemically reactive and the $[Pt_2]^0$ to be the most stable one among the three chosen dimers.
2. Individual adsorption energies of the reactants are found to be highest for the $[Pt_2]^+$ dimer whereas the co-adsorption energy of NO and O_2 is highest for the anionic system. Adsorption analysis further advocates that the co-adsorption energy values of two NO molecules on the catalyst is more negative than those of NO and O_2 and two O_2 molecules.
3. Based on the co-adsorption energies of all the three dimers, the bimolecular L-H mechanism and two trimolecular TER and TLH mechanisms have been considered. Owing to the greater co-adsorption energy of two NO molecules, the probability of reactions occurring via trimolecular reactions is higher.
4. For L-H mechanism, it can be pointed out that the formation of two NO_2 molecules is feasible only in the $[Pt_2]^+$catalyst via LH-1. Whereas the activation barrier for the formation of second NO_2 (TS3n, TS3c, TS3a) via LH-2 is measured to be high in all the systems.
5. Three different TER mechanisms (TER-1, TER-2 and TER-3) were proposed, in which the TER-3 mechanism is found to be more feasible for catalysing 2 NO to 2 NO_2 on $[Pt_2]^-$ dimer, owing to its low activation barriers. For TLH mechanism, $[Pt_2]^0$ dimer is found to be more effective.
6. Overall, it can be concluded that the new TER mechanism (TER-3) is the most efficient pathway for the conversion of two NO to NO_2 molecules on $[Pt_2]^-$ dimer using molecular O_2. Additionally, it was observed that reaction temperature has a promoting effect on the reaction rate of the oxidation mechanism.

7. The present study explores the oxidation process of NO to NO_2 at the atomistic level and shed light on the importance of relatively less explored models of trimolecular chemical reactions as such. We hope the present work might provide a point of reference for future theoretical and experimental studies on catalytic oxidation processes using small transition metal clusters.

3.5 Bibliography

[1] Reşitoğlu, İ. A., Altinişik, K., and Keskin, A. The pollutant emissions from diesel-engine vehicles and exhaust aftertreatment systems. *Clean Technologies and Environmental Policy*, 17:15-27, 2015.

[2] Najjar, Y. S. Gaseous pollutants formation and their harmful effects on health and environment. *Innovative energy policies*, 1:1-9, 2011.

[3] Du, X., Bai, M., Chen, Y., and Huang, Y. Flower-like CuO/CeO_2-NiO microspheres catalysts for the NO reduction by CO: Significant promoting effect of nickel. *Materials Letters*, 275:128083, 2020.

[4] Dhal, G.C., Mohan, D., and Prasad, R. Preparation and application of effective different catalysts for simultaneous control of diesel soot and NO_x emissions: An overview. *Catalysis Science & Technology*, 7:1803-1825, 2017.

[5] Li, L., Shen, Q., Cheng, J., and Hao, Z. Catalytic oxidation of NO over TiO_2 supported platinum clusters I. Preparation, characterization and catalytic properties. *Applied Catalysis B: Environmental*, 93:259-266, 2010.

[6] Enger, B. C., Auvray, X., Lødeng, R., Menon, M., Waller, D., and Rønning, M. Catalytic oxidation of NO to NO_2 for nitric acid production over a Pt/Al_2O_3 catalyst. *Applied Catalysis A: General*, 564:142-146, 2018.

[7] Olsson, L. and Fridell, E. The influence of Pt oxide formation and Pt dispersion on the reactions $NO_2 \Leftrightarrow$ NO+ 1/2 O_2 over Pt/Al_2O_3 and Pt/BaO/Al_2O_3. *Journal of Catalysis*, 210:340-353, 2002.

[8] Smeltz, A. D., Getman, R. B., Schneider, W. F., and Ribeiro, F. H. Coupled theoretical and experimental analysis of surface coverage effects in Pt-

catalyzed NO and O_2 reaction to NO_2 on Pt (1 1 1). *Catalysis Today*, 136:84-92, 2008.

[9] Schmitz, P. J., Kudla, R. J., Drews, A. R., Chen, A. E., Lowe-Ma, C. K., McCabe, R. W., Schneider, W. F., and Goralski Jr, C. T. NO oxidation over supported Pt: Impact of precursor, support, loading, and processing conditions evaluated via high throughput experimentation. *Applied Catalysis B: Environmental*, 67:246-256, 2006.

[10] Crocoll, M., Kureti, S., and Weisweiler, W. Mean field modeling of NO oxidation over Pt/Al_2O_3 catalyst under oxygen-rich conditions. *Journal of catalysis*, 229:480-489, 2005.

[11] Auvray, X. and Olsson, L. Stability and activity of Pd-, Pt-and Pd–Pt catalysts supported on alumina for NO oxidation. *Applied Catalysis B: Environmental*, 168:342-352, 2015.

[12] Mulla, S. S., Chen, N., Cumaranatunge, L., Blau, G. E., Zemlyanov, D. Y., Delgass, W. N., Epling, W. S., and Ribeiro, F. H. Reaction of NO and O_2 to NO_2 on Pt: Kinetics and catalyst deactivation. *Journal of Catalysis*, 241:389-399, 2006.

[13] Denton, P., Giroir-Fendler, A., Praliaud, H., and Primet, M. Role of the Nature of the Support (Alumina or Silica), of the Support Porosity, and of the Pt Dispersion in the Selective Reduction of NO by C_3H_6 under Lean-Burn Conditions. *Journal of Catalysis*, 189:410-420, 2000.

[14] Roduner, E. Size matters: why nanomaterials are different. *Chemical society reviews*, 35:583-592, 2006.

[15] Liu, L. and Corma, A. Metal catalysts for heterogeneous catalysis: from single atoms to nanoclusters and nanoparticles. *Chemical reviews*, 118:4981-5079, 2018.

[16] Böhme, D. K. and Schwarz, H. Gas-phase catalysis by atomic and cluster metal ions: the ultimate single-site catalysts. *Angewandte Chemie International Edition*, 44:2336-2354, 2005.

[17] Cheng, G. J., Zhong, X. M., Wu, Y. D., and Zhang, X. Mechanistic understanding of catalysis by combining mass spectrometry and computation. *Chemical Communications*, 55:12749-12764, 2019.

[18] Wang, T., Ma, J., Yin, B., and Xing, X. Adsorption of O_2 on anionic gold clusters in the 0–1 nm size range: an insight into the electron transfer dynamics from kinetic measurements. *The Journal of Physical Chemistry A*, 122:3346-3352, 2018.

[19] Luo, Z., Castleman Jr, A. W., and Khanna, S. N. Reactivity of metal clusters. *Chemical reviews*, 116:14456-14492, 2016.

[20] Fernandez, E., Liu, L., Boronat, M., Arenal, R., Concepcion, P., and Corma, A. Low-temperature catalytic NO reduction with CO by subnanometric Pt clusters. *ACS catalysis*, 9:11530-11541, 2019.

[21] Weiss, B. M. and Iglesia, E. NO oxidation catalysis on Pt clusters: elementary steps, structural requirements, and synergistic effects of NO_2 adsorption sites. *The Journal of Physical Chemistry C*, 113:13331-13340, 2009.

[22] Xu, Y., Getman, R. B., Shelton, W. A., and Schneider, W. F. A first-principles investigation of the effect of Pt cluster size on CO and NO oxidation intermediates and energetics. *Physical Chemistry Chemical Physics*, 10:6009-6018, 2008.

[23] Narula, C. K., Allard, L. F., Stocks, G. M., and Moses-Debusk, M. Remarkable no oxidation on single supported platinum atoms. *Scientific Reports*, 4:7238, 2014.

[24] Hamad, B., El-Bayyari, Z., and Marashdeh, A. Investigation of the stability of platinum clusters and the adsorption of nitrogen monoxide: First principles calculations. *Chemical Physics*, 443:26-32, 2014.

[25] Li, L., Cheng, J., and Hao, Z. Catalytic oxidation of NO over TiO_2 supported platinum clusters. II: Mechanism study by in situ FTIR spectra. *Catalysis Today*, 158:361-369, 2010.

[26] Bhatia, D., McCabe, R. W., Harold, M. P., and Balakotaiah, V. Experimental and kinetic study of NO oxidation on model Pt catalysts. *Journal of Catalysis*, 266:106-119, 2009.

[27] Tang, Y., Chen, W., Zhao, G., Teng, D., Cui, Y., Li, Z., Feng, Z., and Dai, X. Comparative Study of NO and CO Oxidation Reactions on Single-Atom Catalysts Anchored Graphene-like Monolayer. *ChemPhysChem*, 22:606-618, 2021.

[28] Tang, Y., Zhou, J., Chen, W., Chai, H., Li, Y., Feng, Z., and Dai, X. Theoretical evaluation on single-atom Fe doped divacancy graphene for catalytic CO and NO oxidation by O_2 molecules. *Molecular Catalysis*, 476:110524, 2019.

[29] Zhu, C., Liang, J. X., Wang, Y. G., and Li, J. Non-noble metal single-atom catalyst with MXene support: Fe_1/Ti_2CO_2 for CO oxidation. *Chinese Journal of Catalysis*, 43:1830-1841, 2022.

[30] Meier, M., Hulva, J., Jakub, Z., Kraushofer, F., Bobić, M., Bliem, R., Setvin, M., Schmid, M., Diebold, U., Franchini, C., and Parkinson, G. S. CO oxidation by Pt_2/Fe_3O_4: Metastable dimer and support configurations facilitate lattice oxygen extraction. *Science Advances*, 8:p.eabn4580, 2022.

[31] Yan, H., Lin, Y., Wu, H., Zhang, W., Sun, Z., Cheng, H., Liu, W., Wang, C., Li, J., Huang, X., and Yao, T. Bottom-up precise synthesis of stable platinum dimers on graphene. *Nature communications*, 8:1070, 2017.

[32] Gong, X. Q., Selloni, A., Dulub, O., Jacobson, P., and Diebold, U. Small Au and Pt clusters at the anatase TiO_2 (101) surface: behavior at terraces, steps, and surface oxygen vacancies. *Journal of the American Chemical Society*, 130:370-381, 2008.

[33] Mon, M., Rivero-Crespo, M. A., Ferrando-Soria, J., Vidal-Moya, A., Boronat, M., Leyva-Pérez, A., Corma, A., Hernández-Garrido, J. C., López-Haro, M., Calvino, J. J., and Ragazzon, G. Synthesis of densely packaged, ultrasmall Pt^0_2 clusters within a thioether-functionalized MOF: catalytic activity in industrial reactions at low temperature. *Angewandte Chemie*, 130:6294-6299, 2018.

[34] Wang, F., Zhang, D., Xu, X., and Ding, Y. Theoretical study of the CO oxidation mediated by Au_3^+, Au_3, and Au_3^-: mechanism and charge state effect of gold on its catalytic activity. *The Journal of Physical Chemistry C*, 113:18032-18039, 2009.

[35] Bhattacharjee, D., Mishra, B. K., Chakrabartty, A. K., and Deka, R. C. Catalytic activity of anionic Au–Ag dimer for nitric oxide oxidation: a DFT study. *New Journal of Chemistry*, 39:2209-2216, 2015.

[36] Muramatsu, S. and Tsukuda, T. Reductive Activation of Small Molecules by Anionic Coinage Metal Atoms and Clusters in the Gas Phase. *Chemistry–An Asian Journal*, 14:3763-3772, 2019.

[37] Frisch, M. J., Trucks, G. W., Schlegel, H. B., Scuseria, G. E., Robb, M. A., Cheeseman, J. R., Scalmani, G., Barone, V., Mennucci, B., Petersson, G. A., Nakatsuji, H., Li, X., Caricato, M., Marenich, A. V., Bloino, J., Janesko, B. G., Gomperts, R., Mennucci, B., Hratchian, H. P., Ortiz, J. V., Izmaylov, A. F., Sonnenberg, J. L., Williams-Young, D., Ding, F., Lipparini, F., Egidi, F., Goings, J., Peng, B., Petrone, A., Henderson, T., Ranasinghe, D., Zakrzewski, V. G., Gao, J., Rega, N., Zheng, G., Liang, W., Hada, M., Ehara, M., Toyota, K., Fukuda, R., Hasegawa, J., Ishida, M., Nakajima, T., Honda, Y., Kitao, O., Nakai, H., Vreven, T., Throssell, K., Montgomery, J. A. Jr., Peralta, J. E., Ogliaro, F., Bearpark, M. J., Heyd, J. J., Brothers, E. N., Kudin, K. N., Staroverov, V. N., Keith, T. A., Kobayashi, R., Normand, J., Raghavachari, K., Rendell, A. P., Burant, J. C., Iyengar, S. S., Tomasi, J., Cossi, M., Millam, J. M., Klene, M., Adamo, C., Cammi, R., Ochterski, J. W., Martin, R. L., Morokuma, K., Farkas, O., Foresman, J. B., Fox, D. J. Gaussian 09, Revision D. 01, Gaussian, Inc., Wallingford CT, 2009.

[38] Zhao, Y. and Truhlar, D. G. A new local density functional for main-group thermochemistry, transition metal bonding, thermochemical kinetics, and noncovalent interactions. *The Journal of chemical physics*, 125:194101, 2006.

[39] Weigend, F. and Ahlrichs, R. Balanced basis sets of split valence, triple zeta valence and quadruple zeta valence quality for H to Rn: Design and assessment of accuracy. *Physical Chemistry Chemical Physics*, 7:3297-3305, 2005.

[40] Du, J., Sun, X., and Wang, H. The confirmation of accurate combination of functional and basis set for transition-metal dimers: Fe_2, Co_2, Ni_2, Ru_2, Rh_2, Pd_2, Os_2, Ir_2, and Pt_2. *International Journal of Quantum Chemistry*, 108:1505-1517, 2008.

[41] Lide D. R. *CRC handbook of chemistry and physics*, CRC Press, New York, 89th edition, 2009.

[42] Biswakarma, N., Sarma, P. J., Baruah, S. D., Gour, N. K., and Deka, R. C. Catalytic oxidation of NO on $[Au–M]^-$(M= Pd and Pt) bimetallic dimers: an insight from density functional theory approach. *The Journal of Physical Chemistry C*, 124:3059-3068, 2020.

[43] Maitarad, P., Namuangruk, S., Zhang, D., Shi, L., Li, H., Huang, L., Boekfa, B., and Ehara, M. Metal–porphyrin: a potential catalyst for direct decomposition of N_2O by theoretical reaction mechanism investigation. *Environmental science & technology*, 48:7101-7110, 2014.

[44] Boekfa, B., Treesukol, P., Injongkol, Y., Maihom, T., Maitarad, P. and Limtrakul, J., 2018. The activation of methane on Ru, Rh, and Pd decorated carbon nanotube and boron nitride nanotube: a DFT study. Catalysts, 8:190, 2018.

[45] Ferrighi, L., Hammer, B., and Madsen, G. K. 2D− 3D transition for cationic and anionic gold clusters: a kinetic energy density functional study. *Journal of the American Chemical Society*, 131:10605-10609, 2009.

[46] Biswakarma, N., Dowerah, D., Baruah, S. D., Sarma, P. J., Gour, N. K., and Deka, R. C. Catalytic oxidation of NO to NO_2 on pure and doped Au_nPt_{3-n} (n= 0–3) clusters: A DFT perspective. *Molecular Catalysis*, 515:111910, 2021.

[47] Schlegel, H. B. Optimization of equilibrium geometries and transition structures. *Journal of computational chemistry*, 3:214-218, 1982.

[48] Peng, C. and Bernhard Schlegel, H. Combining synchronous transit and quasi-newton methods to find transition states. *Israel Journal of Chemistry*, 33:449-454, 1993.

[49] Gonzalez, C. and Schlegel, H. B. Improved algorithms for reaction path following: higher-order implicit algorithms. *The Journal of chemical physics*, 95:5853-5860, 1991.

[50] Kestner, N. R. and Combariza, J. E. Basis set superposition errors: Theory and practice. *ReViews in computational chemistry*, 99-132, 1999.

[51] Foster, J. P. and Weinhold, F. Natural hybrid orbitals. *Journal of the American Chemical Society*, 102:7211-7218, 1980.

[52] Lu, T. and Chen, F. Multiwfn: A multifunctional wavefunction analyzer. *Journal of computational chemistry*, 33:580-592, 2012.

[53] Laidler, K. J. *Chemical Kinetics*, Pearson Education, 3rd edition, 2008.

[54] Ončák, M., Cao, Y., Beyer, M. K., Zahradník, R., and Schwarz, H. Gas-phase reactivities of charged platinum dimers with ammonia: A combined experimental/theoretical study. *Chemical Physics Letters*, 450:268-273, 2008.

[55] Cheng, J. and Hu, P. Utilization of the three-dimensional volcano surface to understand the chemistry of multiphase systems in heterogeneous catalysis. *Journal of the American Chemical Society*, 130:10868-10869, 2008.

[56] Wiberg, K. B. Application of the pople-santry-segal CNDO method to the cyclopropylcarbinyl and cyclobutyl cation and to bicyclobutane. *Tetrahedron*, 24:1083-1096, 1968.

[57] Xu, S., Wang, C., and Cui, Y. Theoretical study on influence of ligand and solvent to CdS clusters. *International Journal of Quantum Chemistry*, 111:156-164, 2011.

[58] Mecheri, S. and Zouchoune, B. Terminal and bridging ligand effects on M(I)-M(I) multiple bonding: A DFT investigation of the coordination in (X)[M_2Cl] L_2 complexes (M= Cr, Fe, L= CO, PEt_3, X= Cl, allyl, Cp, and indenyl). *International Journal of Quantum Chemistry*, 123:e27089, 2023.

[59] Yang, W., Gao, Z., Liu, X., Li, X., Ding, X., and Yan, W. Single-atom iron catalyst with single-vacancy graphene-based substrate as a novel catalyst for NO oxidation: a theoretical study. *Catalysis Science & Technology*, 8:4159-4168, 2018.

[60] Gao, Z., Li, A., Liu, X., Ma, C., Li, X., Yang, W., and Ding, X. Density functional study of the adsorption of NO on Ni_n (n= 1, 2, 3 and 4) clusters doped functionalized graphene support. *Applied surface science*, 481:940-950, 2019.

[61] Liu, X., Gao, Z., Huang, H., Yan, G., Huang, T., Chen, C., Yang, W., and Ding, X. L. Simultaneous catalytic oxidation of nitric oxide and elemental mercury by single-atom Pd/g-C_3N_4 catalyst: A DFT study. *Molecular Catalysis*, 488:110901, 2020.

[62] Begum, P., Gogoi, P., Mishra, B. K., and Deka, R. C. Theoretical insight of nitric oxide adsorption on neutral and charged Pd_n (n= 1–5) clusters. *International Journal of Quantum Chemistry*, 115:837-845, 2015.

[63] Cheng, Y., Shi, S., Song, Y., Liu, B., Yao, C., Jiang, J., Li, Y., and Chen, D. Density functional theory study of the adsorption of NO on Cu_nX (n= 2–8; X= Cu, K) clusters. *International Journal of Quantum Chemistry*, 124:e27289, 2024.

[64] Olsson, L., Persson, H., Fridell, E., Skoglundh, M., and Andersson, B. A kinetic study of NO oxidation and NO_x storage on Pt/Al_2O_3 and Pt/BaO/Al_2O_3. *The Journal of Physical Chemistry B*, 105:6895-6906, 2001.

[65] Torres, D., González, S., Neyman, K. M., and Illas, F. Adsorption and oxidation of NO on Au (1 1 1) surface: Density functional studies. *Chemical physics letters*, 422:412-416, 2006.

[66] Gao, Z., Liu, X., Li, A., Li, X., Ding, X., and Yang, W. Bimetallic sites supported on N-doped graphene ((Fe, Co)/N-GN) as a new catalyst for NO oxidation: A theoretical investigation. *Molecular Catalysis*, 470:56-66, 2019.

[67] Yang, W., Feng, Y., Chen, X., Wu, C., Wang, F., Gao, Z., Liu, Y., Ding, X., and Li, H. Understanding Trends in the NO Oxidation Activity of Single-Atom Catalysts. *Journal of Environmental Chemical Engineering*, 10:108744, 2022.

[68] Ovesson, S., Lundqvist, B. I., Schneider, W. F., and Bogicevic, A. NO oxidation properties of Pt (111) revealed by ab initio kinetic simulations. *Physical Review B—Condensed Matter and Materials Physics*, 71:115406, 2005.

[69] Edwards, P. M. Origin 7.0: scientific graphing and data analysis software. *Journal of chemical information and computer sciences*, 42:1270-1271, 2002.